Operator Adjustable Impedance in Bilateral Remote Manipulation

by

G. Jagannath Raju

Bachelor of Technology in Mechanical Engineering
Indian Institute of Technology at Madras
(1977)

Master of Science in Mechanical Engineering
University of California at Berkeley
(1979)

Mechanical Engineer
Massachusetts Institute of Technology
(1985)

SUBMITTED TO THE DEPARTMENT OF
MECHANICAL ENGINEERING
IN PARTIAL FULFILLMENT OF THE REQUIREMENTS
FOR THE DEGREE OF

DOCTOR OF SCIENCE in MECHANICAL ENGINEERING

at the
Massachusetts Institute of Technology
September 1988

Signature of Author. . .
Department of Mechanical Engineering
September 1988

Certified by. . . . . .
Thomas B. Sheridan
Thesis Supervisor

Accepted by. . . . . .
Ain A. Sonin
Chairman, Department Committee

Operator Adjustable Impedance in

Bilateral Remote Manipulation

by

G. Jagannath Raju

Submitted to the Department of Mechanical Engineering

on September 23, 1988 in partial fulfillment of the

requirements for the Degree of Doctor of Science in

Mechanical Engineering

Abstract

A 2-port impedance network model of a single degree of freedom remote manipulation system in which a human operator at the master port interacts with a task object at the slave port in a remote location is presented. The design of the network involves the selection of feedback gains for the servomechanisms that transmit motion and force information from one port of the 2-port to the other in both directions. The methodology proposed here allows for this selection to be based on both stability requirements and specifications of desired port impedances given models of the task and the human operator. The resulting design guidelines guarantee stability for any passive task object at the slave port and any passive human impedance at the master port. Experimental results with an example task are presented.

Thesis Supervisor: Dr. Thomas B. Sheridan

Professor of Mechanical Engineering and Applied Psychology

Dedicated to my parents

Lalita and Krishnamurthy

Acknowledgements

This work was supported in part by the Jet Propulsion Laboratory under Contract No. 956892. I would like to thank Dr. Antal Becjzy at JPL for his encouragement and support over the duration of the project.

One of the benefits of a "tenured" graduate student status is the opportunity to interact with many faculty, staff and students in the institute. Prof. Tom Sheridan provided me with funding and moral support and patiently awaited this document for many years. Thank you, Tom. Thanks also to Prof. Neville Hogan for taking the time to discuss many of the key elements of this thesis and providing many relevant references. I had the pleasure of being a teaching assistant to Prof. Paul Houpt and to Prof. Derek Rowell. Thank you, Derek, for being a teacher, and a friend when my spirits needed uplifting. I could always count on Prof. Will Durfee for help and advice both as a colleague and as a faculty member, and for improving my tennis game. Prof. Kamal Youcef-Toumi and Fawzia Youcef-Toumi have been part of my extended family since my arrival at M.I.T. and have always been a source of comfort and support. Bob Samuel in the Student Machine Shop provided all the machining assistance I needed to construct the hardware, in addition to unsolicited advice on other matters.

Over many years my colleagues in the Man-Machine Systems Lab have provided the sustenance, companionship and support that is essential to endure the experience. Thanks are due in particular to Dana Yoerger and Ahmet Buharali, the original team and still going strong; John Schneiter, for help at the early stages of this work; Hami Kazerooni, for many volatile discussions on impedance control; Jim Roseborough, a true soul-mate; Sam and Mija Landsberger, a home away from home; Hari Das, the proverbial old reliable; Leon Charny, for constantly boosting my ego with kind words; Forrest Buzan, for listening patiently to my musings on life; Max Mendel, for exploring with me all the local eating places; and Chin Kan-Ping, for reading some of my early reports and helping with the experiments. I would also like to thank Ren Jie, Cheng Chi-Cheng, Wael Yared, and Jong Park for their friendship.

Jim Kottas helped me design and debug the electronics, and shared my interests in photography and cycling. Thanks are due to Mrs. Catherine Webb, and her family, for making me feel at home for the past six years. Ron Mayville was a constant source of encouragement and a true friend in times of need.

Behind every doctorate is a "guru", whose wisdom and guidance form the foundation on which a thesis can be constructed. Prof. George Verghese is a "guru" in every sense of the word and more. The time and effort that he spent in answering my queries, providing references, suggesting approaches and solutions, reading all my drafts and making copious comments, improvements, and enhancements, culminated in the completion of this thesis. Thank you, George, and may your tribe increase!

CONTENTS

LIST OF FIGURES

LIST OF TABLES

1. Introduction

The field of telemanipulation has grown by leaps and bounds in the past four decades and promises to continue on this path, as humans pursue the exploration of the vast environs of space, and the depths of the oceans. What began more than forty years ago in a nuclear research lab as a safe means of handling radioactive fuel has now developed into a field that can be concisely described by one word - "tele-presence". I would like to feel that I am "there" without "being" there. The motivations are primarily safety and cost. We can mine coal without descending through unsafe shafts. Sunken treasures can be recovered with lower risks of suffering a similar fate. A malfunctioning satellite can be fixed by a ground-based team of troubleshooters. The common thread that links all these scenarios is the desire to project our functionality as humans to hazardous and/or remote locations while minimizing any associated risks. It is to a small part of this field of research that this thesis hopes to make a contribution.

1.1 Background

The concept of using a manipulator to handle tasks in hazardous environments goes back to the 1940s when master-slave manipulators (MSMs) were designed at the Argonne National Laboratory[1] to handle radioactive nuclear

fuel in hot-cells. A master-slave-manipulator consists of a master arm mounted in a safe location and connected to a slave arm in the remote area. Early designs used mechanical linkages to transmit rotations of the master arm joints to the corresponding joints on the slave arm. Metallic tapes or cables wound around the master arm joints were fed through a tube to the slave arm in the hot cell. Since such a linkage required that the through-tube not be completely sealed, the hot cell had to be maintained at a lower pressure than the surroundings. Another constraint imposed by mechanical linkages was that the distance between the master and slave arms had to be short and fixed.

As handling requirements became more complex, the mechanical arms gave way to servo-driven electro-mechanical arms that had the added capability of providing the human operator with an improved sense of the forces of interaction with the object being handled, and also removed the restriction of the distance between the master and slave arms imposed by the mechanical linkages. Electrical motors were used as actuators to drive the slave arm joints, with the actuator signal based on measurements of the slave and master arm joint angles and velocities. In addition, electrical motors were mounted on the master arm joints and driven by the same joint angle and velocity error measurements to synthesize a force-feedback to the human operator handling the master arm. Performance levels[2] using these force-feedback MSMs improved significantly and attracted attention from other people engaged in remote manipulation tasks.

Two natural areas for applying this teleoperator[1] technology were in the two directions that explorers headed, down into the oceans and up into space. One interesting application of remote manipulators was in 1966 when a nuclear bomb that had accidentally(!!) fallen into the Mediterranean Sea was located by ALVIN (a manned underwater submersible operated by the Woods Hole Oceanographic Institute in Woods Hole, Massachusetts, U.S.A.) and recovered using the CURV (Cable-controlled Underwater Research Vehicle) Teleoperator developed by the Naval Ocean Systems Center (NOSC) in San Diego[3]. At present the Deep Submergence Lab at Woods Hole is engaged in a project for underwater exploration called the Argo-Jason project [4] that will use teleoperator arms mounted on submersibles.

In space applications the Canadian-built arm mounted on the NASA space shuttles has been used to pluck malfunctioning satellites from space for repair[5] in the shuttle cargo bay. To reduce the level of EVA (Extra-Vehicular Activity) for astronauts aboard the space shuttle, NASA plans to deploy free-flying, autonomous, telerobotic vehicles for construction, maintenance, inspection and repair of the Space Station and satellites[6] [7] [8]. Most of the proposed designs[9] [10] of such a telerobotic servicer envisage a twin-arm, one-legged teleoperator garaged in the shuttle that will fly out to the worksite, attach itself to the worksite by its

1. I will use the term 'teleoperator' to represent a manipulator in a remote location, and the term 'master-slave manipulator' to represent a pair of manipulator arms, the slave at the remote end, and the master at the operator end.

single stabilizer leg and carry out the task autonomously, under supervisory control from an astronaut aboard the shuttle, or possibly from personnel at the flight control center on earth.

There are now a few commercial firms marketing manipulator arms constructed of high-strength light-weight materials, and using advanced microcircuit technology for computer control, aimed primarily at the undersea vehicle market. There exists a vast field of possible applications for this technology. As the search for mineral wealth and food resources expands to the ocean floor and the danger to divers increases with depth (in addition to decreasing productivity owing to greater times needed for depressurization), manipulators mounted on submersibles seem to offer an attractive alternative, though economic feasibility is yet unproven.

Whether it be in space, underwater or underground, the future applications of teleoperators for remote manipulation seem numerous and promising.

1.2 Issues in remote manipulation

When humans manipulate objects in their environment, two senses that are extensively used are vision and the "muscle senses" that mediate kinesthesis and proprioception. Sometimes skin senses that mediate pressure and temperature are useful. The assumption made here is that the objective of the manipulation task is to identify and/or alter the location of an object in the environment. The

ultimate goal in remote manipulation would be the complete transparency of the interface, i.e., the actuators that transmit the command and the sensors that return the required information. The term "telepresence" reflects this concept of transporting the human operator not in body but in sensation to the remote location. Though the "skin senses" may be blocked by a telemanipulator mechanism and/or the telecommunication channel, the "muscle senses" and vision may be replaced with high fidelity transmission channels of vision and force/displacement. In reality, owing to limitations imposed by the environment (distances, transmission medium) and technology (sensor resolution, transmission bandwidth, time delays) the transmission signals are degraded and have to be enhanced or compensated for in some way to be of real value.

Many researchers[2] have attempted to enhance the visual images obtained from video feedback using some novel techniques. Research into similarly enhancing the fidelity of force transmission channels has picked up over the past few years. A force feedback channel can provide the operator with values of the force levels in the interaction with the object, displayed on a screen, or better still convert these measurements back to a force level through a servo-actuator to redirect a sense of "feel" to the operator. The force transmission channel in the forward direction transmits the forces that the human operator would have

2. See the section on Sensing and Perception of Volume 2 of the Proceedings of the Workshop on Space Telerobotics edited by G. Rodriguez, JPL Publication 87-13, July 1987.

imposed on the task had she been able to manipulate the object directly. **The primary objective of this dissertation is to study the effect of allowing the human operator the option to select the dynamics of the force transmission channel to suit personal muscular characteristics and the task being performed in the remote location.** The approach adopted here is to model the MSM as a 2-port network with the operator-master arm interface designated as the master port and the task-slave arm as the slave port. The dynamics of the force transmission channels and the responses of the MSM at the master and slave ports can then be characterized by a set of "network functions".

1.3 Network functions

In electrical network theory the response of a circuit to an excitation signal is characterized by the parameters of the elements that comprise the circuit. These elements may be passive (capacitors, resistors, inductors, transformers, etc.) or active (current or voltage sources). When the excitation signal is a complex sinusoid, the response is also a complex sinusoid of the same frequency for LTI (Linear Time Invariant) systems and the relationship between the excitation signal and the response is represented by a ratio of polynomials that are functions of the complex frequency $s(= \sigma + j\omega)$, where σ is the real part of the complex frequency (also referred to as the neper frequency), and the imaginary part ω is the radian frequency (or sometimes referred to as the real frequency, not to be confused with the real part of the complex frequency) of the excitation signal.

This rational function that relates the excitation signal with the measured response is called the network function $N(s)$.

$$N(s) = \frac{\sum_{j=0}^{m+1} a_j s^j}{\sum_{k=0}^{n+1} b_k s^k} = \frac{\prod_{j=0}^{m} (s - z_j)}{\prod_{i=0}^{n} (s - p_i)}$$

where z_j and p_i are the zeros ($N(s)=0$ for $s=z_j$) and poles ($N(s)=\infty$ for $s=p_i$) of the transfer function. Since the response to an excitation signal applied at one node of the network can be measured at the same node or at other nodes, the network function can take on different forms. When the excitation signal is a voltage and the measured response is a current the network function is called an *admittance*, when the reverse is true, it is called an *impedance*. The term *immitance* is used to refer to a network function that is either an impedance or an admittance.

If the immitance relates the response to the excitation at the same node where the excitation (or driving) signal is applied, it is called a driving point immitance, else it is called an immitance transfer function. For the case when the excitation signal at one node and the response at another node are both voltages or both currents, the network function is called a voltage transfer function or a current transfer function respectively. It should be noted that for LTI systems, the driving point admittance is the inverse of the driving point impedance, but the same is not generally true for immitance transfer functions.

Force (F) and velocity (V) variables in mechanical systems are analogous to voltage and current signals in electrical networks, so mechanical network functions can be defined similarly. As an example, for a lumped parameter model of a simple mass (M), dashpot (B), spring (K) system, the driving point impedance is:

$$Z(s) = \frac{F(s)}{V(s)} = Ms + B + \frac{K}{s}$$

and hence the driving point admittance is:

$$Y(s) = \frac{1}{Z(s)} = \frac{s}{Ms^2 + Bs + K}$$

1.4 Manipulation by humans

Since the objective of the remote manipulation system is to enable the slave end-effector to manipulate a task object as "skillfully" as a human would,[3] it is enlightening to study the techniques that humans apply in various manipulation tasks, with emphasis on the way a human adjusts the impedance of limbs involved with the task. A few examples are offered below, with an implicit assumption that the ideas presented are for the most part hypothetical in nature and the conclusions drawn are open to debate.

In many sports (racquet sports such as tennis, squash, badminton, table tennis, and other sports such as golf, baseball) the objective is to manipulate the

3. It is relevant to note that there are many tasks that a human cannot execute as easily as a machine can, e.g., tasks that require continuous rotation of more than 360 about an axis.

trajectory of a projectile, usually a spherical ball, using a tool with a passive impedance (a bat, racquet, golf club). The player has two impedances in series that act as a force transmission channel, the active impedance of the human body with emphasis on the limb holding the tool, and the passive impedance of the tool being employed. Players tend to choose tools with impedance characteristics that suit their styles of play, physical attributes, and some other unquantifiable factors.

In tennis, in addition to selecting a racquet by size, weight, inertia and stiffness, players select the tension of the strings to provide control or speed. When the string tension is high (80 lbs) the deformation of the strings on impact with the ball is less than the deformation of the ball and consequently the ball remains in contact with the strings for a longer period of time, providing the player with greater control whilst sacrificing power. On the other hand with lower string tensions (40 lbs) the deformation of the strings is higher, more of the ball's kinetic energy gets stored as potential energy in the strings and the ball rebounds with greater speed. Thus the exchange of power between the racquet and the ball is governed by the two impedances. In addition to selecting the impedance of the racquet the player adjusts the impedance of the arm to suit the stroke being attempted, e.g. for a drop shot at the net the player will lower the arm impedance, effectively absorbing most of the kinetic energy of the ball on impact and thus reducing the rebound speed of the ball.

In baseball, batters have been known to doctor a bat with cork (the tip of the bat is hollowed out and stuffed with cork) to alter its impedance for greater power. In addition, the batter adjusts his arm impedance depending on whether the objective is to swing for a home run or bunt into the infield to get on base.

Golf presents yet another example of a passive tool impedance and an active human impedance in series. In driving off the tee or the fairway, the emphasis is more on transmitting power to the ball on the swing, than on the final position of the ball. In putting, where all the emphasis is on position trajectory control, the arms are held stiffer than while driving.

Since present plans do not envision using remote manipulators to play the World Series underwater or in outer space, a few examples outside the realm of sports and in an industrial assembly context are offered. The peg-in-hole task is the classic example of an assembly task in which it is desirable to have the impedance of the arm inserting the peg (assumed infinitely stiff) low in directions of motion orthogonal to the axis of the hole during insertion of the peg, but have the impedance high along the axis so that enough force can be transmitted to the peg to push it into the hole. A human is able to execute the task by exerting forces in directions in which motion is desired, but allowing the task constraints to determine the motion in the orthogonal directions by offering a low impedance of the arm in those directions. This principle of orthogonality is emphasized by Mason[11] amongst others.

A second task illustrating an instance of humans adjusting arm dynamics is one in which springs of different stiffnesses have to be compressed. When the weaker spring has to be compressed, since the forces required are not high, the arm stiffness need not be high to transmit the force. However when working with the stronger spring, the arm stiffness has to be high enough to transmit the higher force levels.

In all the cases cited, there are two impedances acting in series, one of which is an effective impedance of a human arm with/without a tool, the second being the impedance of the environment being manipulated. The only active impedance is that of the human arm, which is controlled by the nervous system. When the task has to be executed by a manipulator arm, it is logical to attempt to control the impedance at the end-effector to simulate the adaptive arm of a human. Two terms that are extensively used in manipulation research are "force control" and "position control", and the two control objectives may be thought of as specification of a desired impedance of the end-effector to environmental forces. This concept, advanced by Hogan[12] and subsequently adopted by others is a natural way of specifying interaction between coupled dynamic systems. Specification of a maximum position error, a minimum required bandwidth for response, and a maximum or zero overshoot, determines the impedance of the end-effector for position control. For force control, the maximum position error specification is replaced by a maximum force error criterion and a desired end-effector impedance can be computed. Thus force and position control are but two

special cases of a more generalized impedance control.

Some of the early research in compliance control (which can be thought of as a form of admittance control) suggested the use of passive compliance devices at the end-effector to suit particular tasks. Remote-Centered-Compliance (RCC) devices were one example of such tools that were helpful in peg-in-hole insertion tasks. Salisbury[13] suggested the concept of active stiffness control of the end-effector by adapting the feedback control loop of the manipulator joint actuators to provide the desired stiffness of the end-effector to external forces imposed by the task/environment. In such methods the kinematic and dynamic transformations from the joint actuators to the end-effector play a vital role in determining if any desired impedance matrix at the end-effector can actually be achieved by modulating the actuator impedances. Kazerooni [14] [15] addressed some of these issues and developed methods for achieving desired impedances at the robot end-effector. Anderson and Spong[16] propose a combination of hybrid position/force control and impedance control as a strategy to control both the trajectory and the contact forces at a robot's end-effector.

The MSMs built at Argonne National Labs and subsequent models had identical master and slave arms. The primary reason for this configuration was the use of analog servo controllers for the control of the actuators. The necessity of handling heavy loads required that the slave arm had to be strong and stiff. The identical master arm was heavy and difficult for the operator to manuevere. With the advances of computer technology, computer controlled systems were

built which allowed for the master and slave arms to have differing configurations. All the kinematic transformations from master coordinate space to slave coordinate space could now be handled in software. This led researchers to design the master arms to be smaller, lighter and more ergonomic. Such generalized hand controllers[17] [18] [19] allowed development of modular force-feedback systems to which different types of slave arms could be later adapted. Other researchers[20] [21] [22] focused on developing estimation and control methodolgies which could be used to enhance the "feel" that the operator had of the task object primarily by force-feedback. The French Nuclear Industry has invested extensively in computer-aided teleoperation systems[23] [24] [25].

1.5 A remote manipulation system

The sub-systems that comprise a model of a remote manipulation system are depicted in Fig. 1.1.

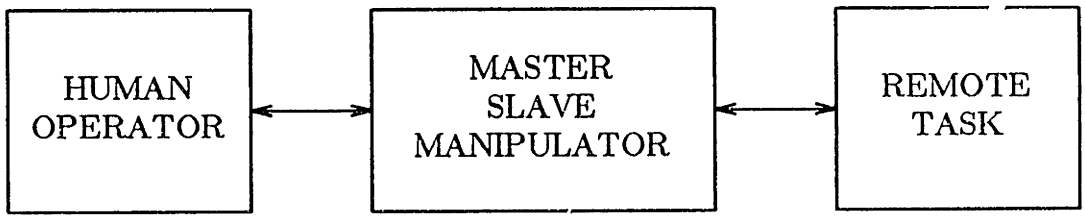

Figure 1.1. Remote manipulation.

The three sub-systems are :

i. the human operator, who manipulates the master device of the MSM in a manner that results in the slave device of the MSM acting on the task to achieve the desired goal;

ii. a MSM which transmits forces and motion between the human operator and the remote task;

iii. the task object in the remote environment that is being manipulated by the slave device of the MSM.

In subsequent chapters models will be presented for the role of each of the sub-systems that comprise a remote manipulation system.

1.6 An ideal telemanipulator

It is relevant to ask at this stage: What constitutes an "ideal" telemanipulator? Intuitively a reasonable response would be: An ideal telemanipulator is one that provides complete transparency of the interface. In other words the operator feels as if the task object were being handled directly. For force-feedback systems Handlykken[18] suggests that this can be represented by an infinitely stiff and weightless mechanical connection between the end-effector of the master arm and the slave arm. Yokokhoji and Yoshikawa[26] argue that the ideal response of a remote manipulator system is one in which the position and force responses of the master arm are systematically equal to the responses of position and force when the operator manipulates the object directly. But from a human factors point of

view, Vertut[23] suggests that the operator may sometimes get tired of holding a constant weight, and reports implementing a system with continuous variation of the force feedback ratio to reduce fatigue and improve precision. Indeed it is not all that clear that the highest level of force-feedback is universally beneficial in executing all tasks. Hill[27] reports that in the classic peg-in-hole insertion task, the insertion phase shows little difference with or without force feedback. Bejczy and Handlykken[28] report from experimental studies that there seems to be an optimal combination of the force-feedback gain (from slave to master) and the feedforward gain (from master to slave) and that this combination may be task dependent.

It appears that as yet there is no consensus regarding an universal idealization of a remote manipulator system. Indeed to some extent the hypothesis in this dissertation is partly motivated by the non-existence of such an universal standard, since this brings out the necessity of designing an adjustable system. An additional implication of this statement may be that the "ideal" telemanipulator is an "adjustable" one.

1.7 Outline of this thesis

Chapter 2 presents the models of the operator and the task, and a 2-port network model of the MSM. In Chapter 3 the hardware that is the realization of the MSM is discussed. Chapter 4 completes the modelling process by presenting a

sampled-data model of the MSM. The stability of the MSM when coupled to the operator at one port and the task at the other is discussed in Chapter 5 along with a design procedure for the selection of the feedback gains. Chapter 6 describes an experiment, and discusses the resulting data. Chapter 7 offers some conclusions and suggestions for further research.

2. Analytical model of the remote manipulation system

In the preceding chapter the human operator's role in manipulation tasks was hypothesized in very qualitative terms. This role manifests itself in two distinct forms, the first in a decision making process, and the second in the application of the decision by motion imposed on the task object. As the objective in the context of this thesis is to determine the power flow between the operator and the master port of the MSM, and its dependence on the physical parameters of the operator's arm, no attempt is made to model the decision making process that the operator uses to alter her arm characteristics. Rather than trying to model any specific limb of the human operator, the approach here will be to attempt to justify the choice of using a linear second-order model to represent the dynamics of the operator's end-effector as seen by the master port of the MSM.

A similar model is also assumed for the task at the slave port. The model for the remaining sub-system, namely the MSM, is developed and combined with the operator and task models to form a model of the overall remote manipulation system.

It will be shown at a later stage that these assumptions about the operator and the task are not as critical as they may seem to be here. If one can realisitically model both the operator and task as passive immitances at the ports, the overall design is simplified. For tasks, most of which are passive in nature, this

approach is reasonable. In the case of models of the human, it appears that active modulation of muscle parameters does occur, a passive model may not be realisitic but may be sufficient in this context.

2.1 Model of human operator

When the operator imposes motion or effort using primarily the upper body, agonist-antagonist pairs of muscles acting primarily about the shoulder, elbow, wrist and finger joints are used. The coupling of many of these pairs of muscles is complex and not of interest here. What is of interest is: what immitance does the operator present to the master port of the MSM?

The first gross assumption will be that the aggregate function of all the muscle pairs that come into play in interacting with the MSM can be lumped into a single muscle pair that exhibits the dynamic behaviour of each pair within the aggregate, but possesses characteristic parameters which account for the sum total effect of all the pairs. This enables us to exploit simple models that describe the dynamics of muscular motion derived from experiments done on isolated muscle.

Reported results[29] [30] [31] from experiments done with isolated muscle fibres (typically from cats and frogs) are shown in Figs. 2.1 and 2.2.[4] In one

4. It should be emphasized that the graphs shown are representative of muscle dynamics only for the purpose of providing a baseline from which a linear model can be approximated. In reality the curves for muscle specimens (from cats, frogs etc.) differ from the graphs shown but can be linearized similarly.

experiment the muscle specimen is held at a constant length and excited, and the tension that develops in the muscle due to the resultant contraction is measured.

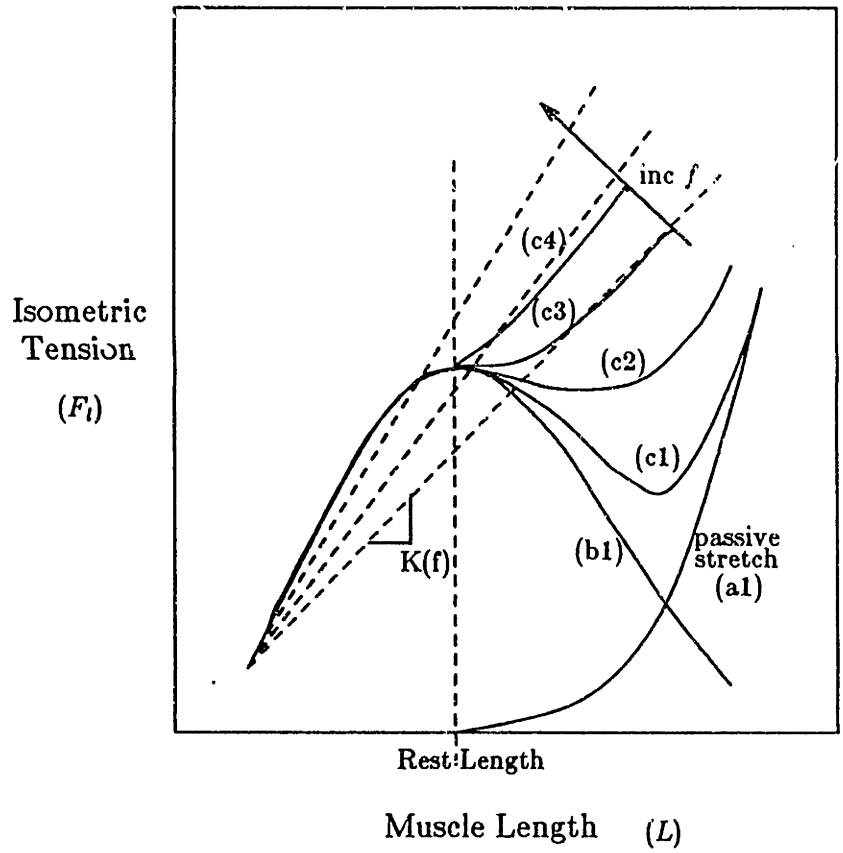

Figure 2.1. Isometric muscle characteristics.

In Fig. 2.1 this isometric tension is plotted against the muscle length for varying frequencies (c1 to c4) of excitation (neural activity level). Each plot has two components, e.g., (c1) comprises a component due to active contraction (b1) and a passive component (a1) due to stretching of the muscle (muscles can only contract actively) beyond its rest length. Muscles seem to develop the maximum tension at about their rest lengths. On approximating (closely following McRuer's

model[32]) the curves with staight lines, the relationship can be modelled as a linear spring with the spring stiffness a function of the excitation frequency :

$$F_l = -K(f)L \tag{2.1}$$

where

f = excitation frequency

L = muscle length

F_l = tension generated in the muscle at length L and firing rate f

$K(f)$ = spring stiffness at excitation frequency f

In another set of experiments the isolated muscle spindle is loaded by a constant weight, and the velocity at which the muscle contracts on excitation is measured. Typical results are shown in Fig. 2.2.

When these curves are approximated by straight lines, the relationship may be represented as

$$\frac{F_v}{P(f)}+\frac{V}{V_m} = 1 \tag{2.2}$$

or

$$F_v = P(f)(1-\frac{V}{V_m}) = P(f)-\frac{P(f)}{V_m}V = P(f)-B(f)V \tag{2.3}$$

where

F_v = load at which muscle is held

$P(f)$ = isometric tension (V=0) at excitation frequency f

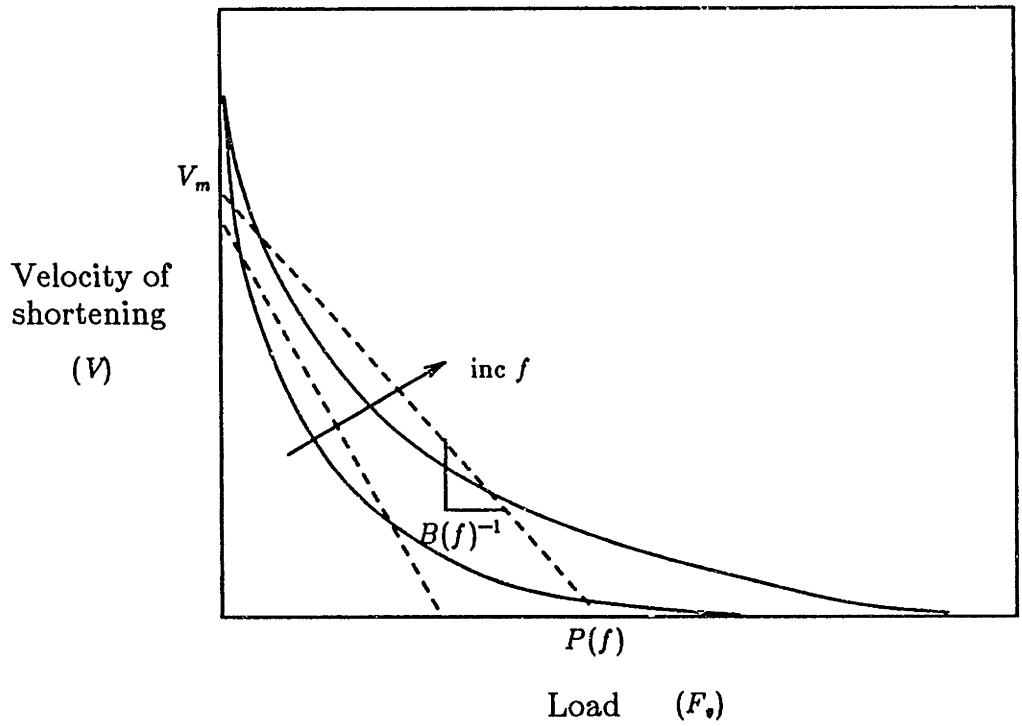

Figure 2.2. Isotonic muscle characteristics.

V_m = maximum shortening velocity

$B(f) = P(f)/V_m$, equivalent damping coefficient

Combining (2.1) and (2.3) to determine the dynamics of muscular motion, the resulting model is

$$F = P(f) - K(f)L - B(f)V \tag{2.4}$$

If the stiffness and damping parameters $K(f)$ and $B(f)$ are selected to represent an aggregate for all the muscle pairs that are used, the dynamics of motion at the human end-effector may be modelled as :

$$J_h \frac{d}{dt}\Omega_h = \textit{Torque exerted by arm - External load} \qquad (2.5)$$
$$= P(f) - K(f)\Theta_h - B(f)\Omega_h - T_{ext}$$

where

Θ_h = operator end-effector position

Ω_h = end-effector velocity

J_h = end-effector inertia

This yields a mass-dashpot-spring model with an effort source $P(f)$ and variable mechanical element parameters.

$$J_h \frac{d}{dt}\Omega_h + B(f)\Omega_h + K(f)\Theta_h = P(f) - T_{ext} = T_{h,f} \qquad (2.6)$$

Assuming a constant nominal firing rate f, the corresponding admittance is

$$Y_h(s) = \frac{1}{Z_h(s)} = \frac{\Omega_h(s)}{T_{h,f}(s)} = \frac{s}{J_h s^2 + B(f)s + K(f)} \qquad (2.7)$$

The operator's arm when viewed from the master end of the MSM appears as an impedance $Z_h(s)$ and an effort source, (equivalent to a voltage source in electrical circuits) $P(f)$.

2.2 Model of remote task

A generalized mass-dashpot-spring model will be used to represent the object being manipulated by the slave arm. Its admittance can thus be represented as

$$Y_t(s) = \frac{1}{Z_t(s)} = \frac{s}{J_t s^2 + B_t s + K_t} \tag{2.8}$$

When viewed from the slave end of the MSM, the task looks like a passive impedance Z_t characterized by its parameters J_t, B_t, K_t (inertia, damping and stiffness).

2.3 Model of master-slave manipulator

The MSM may be modelled as a two-port mechanical system, analogous to two-port electrical networks. At the input or master port, the MSM interacts with the operator; at the output or slave port it interacts with the task object in the remote environment, as illustrated in Fig. 2.3.

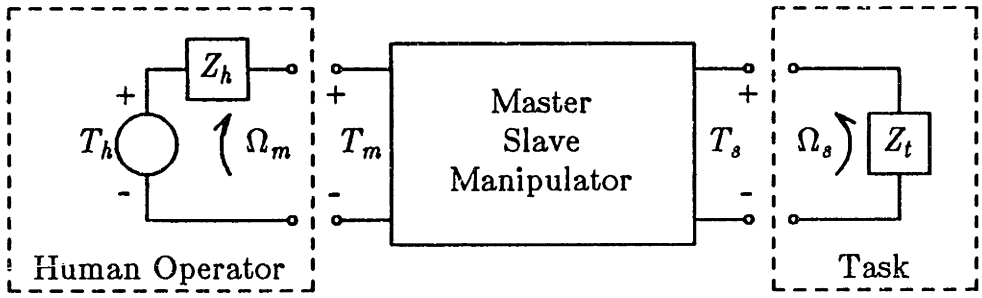

Figure 2.3. Electrical network model of master-slave manipulator

At each port (master and slave) the co-energy variables of interest are the effort variables (torques T_m and T_s) and the flow variables (velocities Ω_m and Ω_s). Either of the co-energy variables at each port may be chosen to be the independent variable, and the value of the dependent variable is then determined by the parameters that characterize the MSM. If the flow variables are considered to be

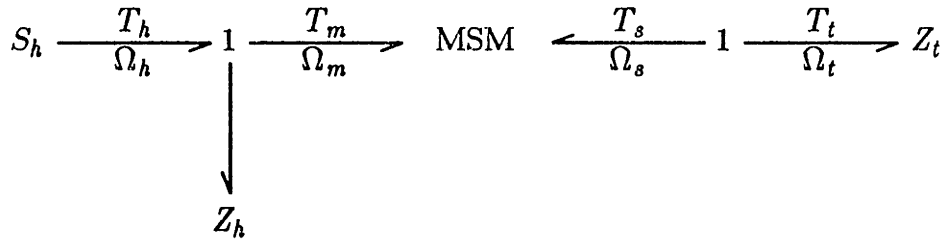

Figure 2.4. Bond graph model of MSM (without causality reference)

the inputs, the MSM can be represented by an impedance matrix $[Z(s)]$ such that

$$\underline{T}(s) = [Z(s)]\,\underline{\Omega}(s) \qquad \underline{T}(s) = \begin{Bmatrix} T_m(s) \\ T_s(s) \end{Bmatrix} \qquad \underline{\Omega}(s) = \begin{Bmatrix} \Omega_m(s) \\ \Omega_s(s) \end{Bmatrix} \tag{2.9}$$

or

$$\begin{Bmatrix} T_m(s) \\ T_s(s) \end{Bmatrix} = \begin{bmatrix} Z_{11}(s) & Z_{12}(s) \\ Z_{21}(s) & Z_{22}(s) \end{bmatrix} \begin{Bmatrix} \Omega_m(s) \\ \Omega_s(s) \end{Bmatrix} \tag{2.10}$$

If, on the other hand, one chooses to specify the inputs to the MSM to be the effort variables, the MSM is represented by an admittance matrix $[Y(s)]$ such that

$$\underline{\Omega}(s) = [Y(s)]\,\underline{T}(s) \tag{2.11}$$

or

$$\begin{Bmatrix} \Omega_m(s) \\ \Omega_s(s) \end{Bmatrix} = \begin{bmatrix} Y_{11}(s) & Y_{12}(s) \\ Y_{21}(s) & Y_{22}(s) \end{bmatrix} \begin{Bmatrix} T_m(s) \\ T_s(s) \end{Bmatrix} \tag{2.12}$$

Two other representations of the MSM are obtained if one of the inputs at one port is an effort variable and the input at the other port is a flow variable, or vice-versa. These are commonly referred to as hybrid models of the 2-port. For example, if the flow is specified at the master port and the effort at the slave port

we get

$$\begin{Bmatrix} T_m(s) \\ \Omega_s(s) \end{Bmatrix} = \begin{bmatrix} H_{11}(s) & H_{12}(s) \\ H_{21}(s) & H_{22}(s) \end{bmatrix} \begin{Bmatrix} \Omega_m(s) \\ T_s(s) \end{Bmatrix} \tag{2.13}$$

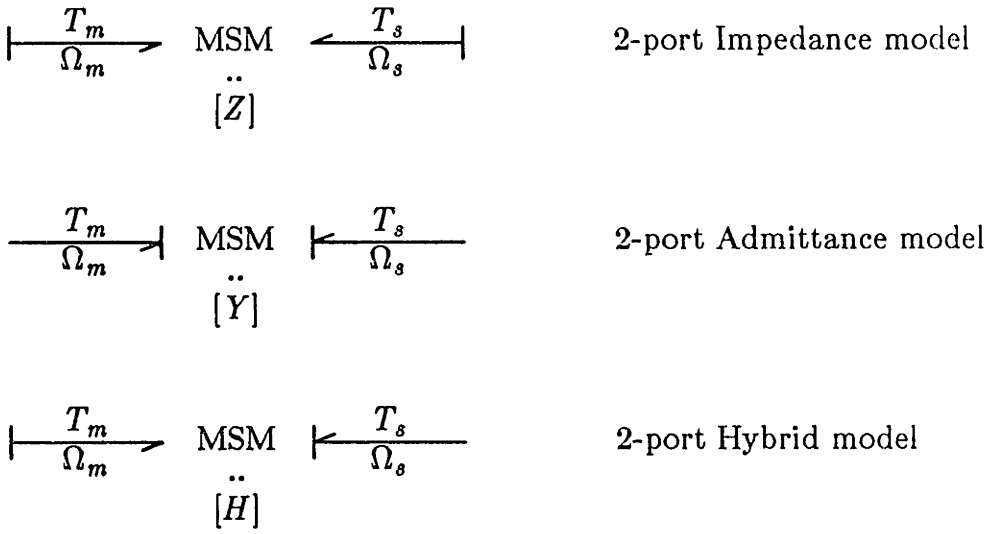

Figure 2.5. Alternative causal models of MSM.

Since each of the preceding representations governs the same physical system, the elements of each matrix can be calculated in terms of the elements of one of the other representations. These relationships can be found in any introductory text on linear circuit theory.[33] [34] [35]

Two special cases of the 2-port that are relevant to our context are the *bilateral* 2-port and the *reciprocal* 2-port. When both the off-diagonal elements of the 2-port matrix are non-zero, signal flow takes place in both directions (state changes at one port cause changes at the other) and the network is called a *bilateral* 2-port. If these two off-diagonal elements are equal the 2-port is termed

reciprocal.

The first step in modelling the MSM is to decide which of the preceding representations is best suited to describing the hardware that comprises the physical MSM. At each port of the physical MSM a servo-actuator is used to generate a control torque based on flow measurements (feedback signals of position and velocity) at both ports. Hence the master and slave servo-actuator control actions can be modelled as dependent torque (effort) sources $U_m\{\Omega_m(s),\Omega_s(s)\}$ and $U_s\{\Omega_m(s),\Omega_s(s)\}$. The control laws for these servo-actuators will be picked so as to obtain an impedance characterization of the MSM, as shown next. A representation of the MSM before imposition of feedback control on the actuators is shown in Fig. 2.6. The dynamics of the master actuator and arm is represented by an impedance $Z_{ma}(s)$, and similarly $Z_{sa}(s)$ represents the dynamics of the slave actuator and arm.

One possible form for the control law is

$$\begin{Bmatrix} U_m(s) \\ U_s(s) \end{Bmatrix} = \begin{bmatrix} -f_{11}(s) & f_{12}(s) \\ f_{21}(s) & -f_{22}(s) \end{bmatrix} \begin{Bmatrix} \Omega_m(s) \\ \Omega_s(s) \end{Bmatrix} \tag{2.14}$$

The sign convention for the diagonal components f_{11} and f_{22} has been chosen to suggest that the response (control) torque at each port should oppose the imposed flow at that port. The torque at the master port is then

$$T_m(s) = Z_{ma}(s)\,\Omega_m(s) - U_m(s)$$

$$= [\, Z_{ma}(s)+f_{11}(s) \,]\, \Omega_m(s) - f_{12}(s)\, \Omega_s(s) \qquad (2.15)$$

Using an identical approach at the slave port yields an impedance matrix that describes the MSM

$$\begin{Bmatrix} T_m(s) \\ T_s(s) \end{Bmatrix} = \begin{bmatrix} Z_{ma}(s)+f_{11}(s) & -f_{12}(s) \\ -f_{21}(s) & Z_{sa}(s)+f_{22}(s) \end{bmatrix} \begin{Bmatrix} \Omega_m(s) \\ \Omega_s(s) \end{Bmatrix} \qquad (2.16)$$

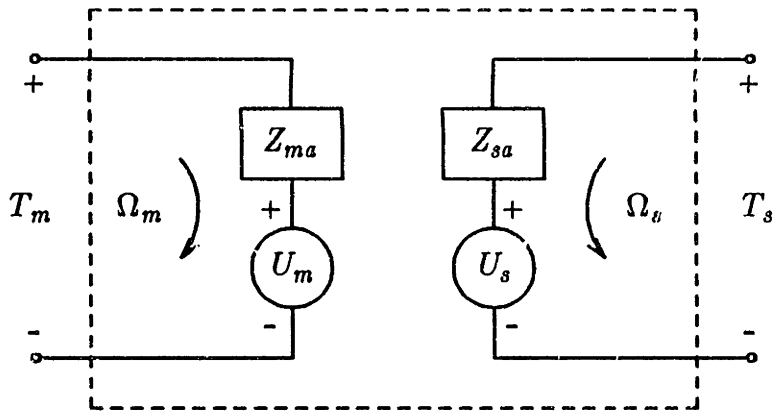

Figure 2.6. MSM port impedances.

The elements of the impedance matrix, i.e. the $Z_{ij}(s)$ are referred to as the *open-circuit impedance parameters* of the two-port network, since they define the effective impedances at the two ports in the absence of loads (the ports are open-circuited). For the MSM these parameters are

$$Z_{11}(s) = \left.\frac{T_m(s)}{\Omega_m(s)}\right|_{\Omega_s(s)=0} = Z_{ma}(s) + f_{11}(s) \qquad (2.17)$$

$$Z_{12}(s) = \left.\frac{T_m(s)}{\Omega_s(s)}\right|_{\Omega_m(s)=0} = -f_{12}(s) \qquad (2.18)$$

$$Z_{21}(s) = \left.\frac{T_s(s)}{\Omega_m(s)}\right|_{\Omega_s(s)=0} = -f_{21}(s) \tag{2.19}$$

$$Z_{22}(s) = \left.\frac{T_s(s)}{\Omega_s(s)}\right|_{\Omega_m(s)=0} = Z_{sa}(s) + f_{22}(s) \tag{2.20}$$

Therefore by proper choice of the elements of the feedback matrix, i.e. the $f_{ij}(s)$, the elements of $[Z(s)]$ can be independently modulated. However, it is not obvious that one can specify these elements intutively; the desired characteristic of the MSM can be expressed more naturally in terms of a master port impedance $Z_m(s)$ presented to the operator, and a slave port impedance $Z_s(s)$ presented to the task. Note that $Z_m(s)$ depends not only on the $Z_{ij}(s)$ but also on the task impedance $Z_t(s)$. Similarly, $Z_s(s)$ depends on the human impedance $Z_h(s)$. Therefore, to find the port impedances $Z_m(s)$ and $Z_s(s)$, the governing equations for the loads at the two ports have to be included. The procedure to determine $Z_s(s)$ is outlined here (and can be found in any linear circuit theory text); $Z_m(s)$ can be derived similarly.

At the master port

$$\begin{aligned} T_h(s) - Z_h(s)\,\Omega_m(s) &= T_m(s) \\ &= Z_{11}(s)\,\Omega_m(s) + Z_{12}(s)\,\Omega_s(s) \end{aligned} \tag{2.21}$$

or

$$\Omega_m(s) = \frac{T_h(s) - Z_{12}(s)\,\Omega_s(s)}{Z_{11}(s) + Z_h(s)} \tag{2.22}$$

Then

$$
\begin{aligned}
T_s(s) &= Z_{21}(s)\,\Omega_m(s) + Z_{22}(s)\,\Omega_s(s) \\
&= Z_{21}(s)\left\{\frac{T_h(s) - Z_{12}(s)\,\Omega_s(s)}{Z_{11}(s) + Z_h(s)}\right\} + Z_{22}(s)\,\Omega_s(s) \\
&= \left\{\frac{Z_{21}(s)}{Z_{11}(s) + Z_h(s)}\right\} T_h(s) + \left\{Z_{22}(s) - \frac{Z_{12}(s)\,Z_{21}(s)}{Z_{11}(s) + Z_h(s)}\right\}\Omega_s(s) \\
&= \left\{\frac{Z_{21}(s)}{Z_{11}(s) + Z_h(s)}\right\} T_h(s) + Z_s(s)\,\Omega_s(s)
\end{aligned}
\tag{2.23}
$$

where

$$
Z_s(s) = Z_{22}(s) - \frac{Z_{12}(s)\,Z_{21}(s)}{Z_{11}(s) + Z_h(s)} \tag{2.24}
$$

The relation (2.23) is depicted in Fig. 2.7.

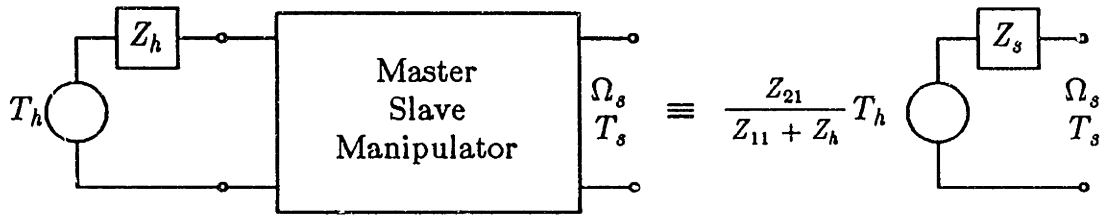

Figure 2.7. Slave port impedance with operator at master port.

Similarly the impedance that the human operator feels at the master port in the presence of a task at the slave port is

$$
Z_m(s) = Z_{11}(s) - \frac{Z_{12}(s)\,Z_{21}(s)}{Z_{22}(s) + Z_t(s)} \tag{2.25}
$$

If the control signals that form the dependent sources are chosen to be non-dynamic linear combinations of the master and slave port positions and velocities, then

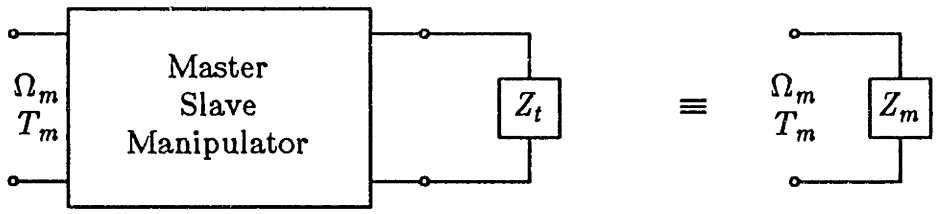

Figure 2.8. Master port impedance with task at slave port.

$$\begin{Bmatrix} U_m(t) \\ U_s(t) \end{Bmatrix} = \begin{bmatrix} -k_{11} & -k_{12} & k_{13} & k_{14} \\ k_{21} & k_{22} & -k_{23} & -k_{24} \end{bmatrix} \begin{Bmatrix} \Theta_m(t) \\ \Omega_m(t) \\ \Theta_s(t) \\ \Omega_s(t) \end{Bmatrix} \tag{2.26}$$

where k_{ij} are the elements of the feedback gain matrix $[K]$.

In the frequency domain this leads to

$$\begin{Bmatrix} U_m(s) \\ U_s(s) \end{Bmatrix} = \begin{bmatrix} -(\frac{k_{11}}{s}+k_{12}) & \frac{k_{13}}{s}+k_{14} \\ \frac{k_{21}}{s}+k_{22} & -(\frac{k_{23}}{s}+k_{24}) \end{bmatrix} \begin{Bmatrix} \Omega_m(s) \\ \Omega_s(s) \end{Bmatrix} \tag{2.27}$$

Then, from (2.14)

$$f_{11}(s) = \frac{k_{11}}{s} + k_{12} \tag{2.28}$$

$$f_{12}(s) = \frac{k_{13}}{s} + k_{14} \tag{2.29}$$

$$f_{21}(s) = \frac{k_{21}}{s} + k_{22} \tag{2.30}$$

$$f_{22}(s) = \frac{k_{23}}{s} + k_{24} \tag{2.31}$$

Thus by modulating the elements of the gain matrix k_{ij}, the elements of the

impedance matrix $[Z(s)]$ can be adjusted to meet desired specifications. Elaboration of this idea is deferred to Chapter 5, with the next two chapters concentrating on further implementation and modeling issues.

The preceding frequency domain analysis of the continuous time signals that describe the dynamics of the MSM provides a structure for the development of a sampled data model of the MSM that more accurately reflects the hardware used to implement the MSM. It is therefore appropriate to introduce the computer controlled actuator system that comprises the MSM in the next chapter before proceeding to a discrete time analysis in the z-domain in Chapter 4.

3. Design of the Master-Slave Experimental System

A single degree-of-freedom Master-Slave Manipulator (MSM) was built to serve as the experimental system for this research work. This section describes the hardware that includes the servo-units and the computer interface that controls the system.

The MSM uses conventional D.C. motors as joint actuators, powered by pulse-width-modulated (PWM) amplifiers. Position and velocity signals are obtained from incremental optical encoders and generator-tachometers that are integrated into the motor units. Fourteen-inch levers that act as the arm links are mounted on collars on the motor shafts, and no gear reduction units are used. The master link arm is equipped with a joystick handle that incorporates three momentary push-button switches and one two-position toggle switch that are intended to be used to adjust the 2-port impedance matrix of the MSM. The PWM amplifiers operate as voltage-to-current amplifiers, thus enabling torque control of the motors that they drive.

An Intel 8 MHz 8086 CPU-based microcomputer with a 8087 Numeric Data Processor is used for computer control of the motors. An IBM-PC Bus based interface card was built to decode the optical encoder signals into signed 16-bit words representing the motor shaft angular positions. This card also provides a programmable Real Time Clock that is used to implement the 60 Hz sampling

frequency. The circuit diagrams for the card are shown in Appendix C.

A Data Acquisition card with 16 Single Ended Analog-to-Digital (A/D) channels, 2 Digital-to-Analog (D/A) channels, and 16 programmable Digital I/O lines is used. Two of the A/D channels are used to sense the angular velocities of the two motors and the two D/A channels to drive the PWM amplifiers with the control signals. The states of the joy-stick switches are monitored by the computer through the Digital I/O lines on the Data Acquisition card. The schematic of the experimental set-up is illustrated in Fig. 3.1. The connections for the various sub-systems are detailed in Appendix B.

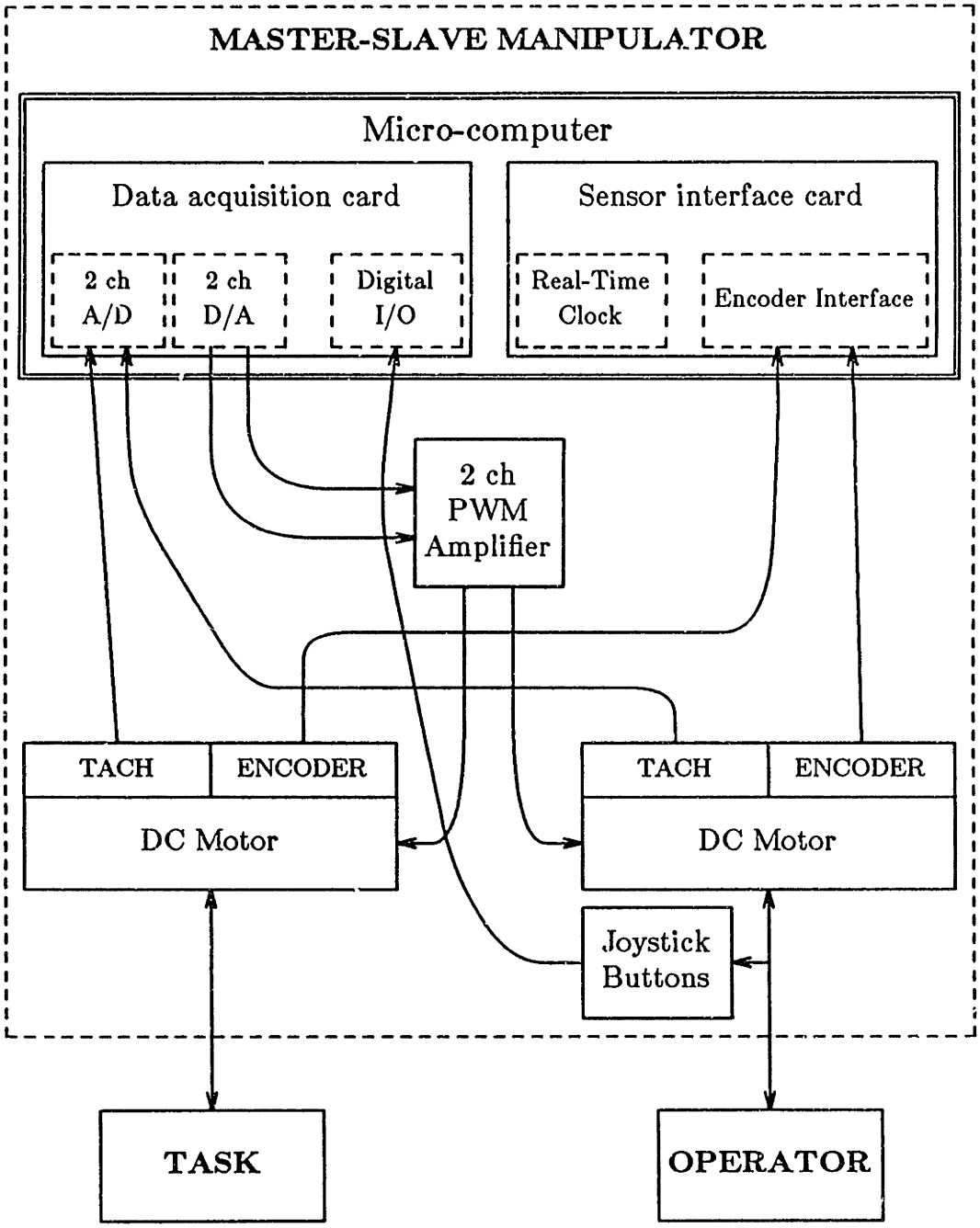

Figure 3.1. Schematic of experimental set-up.

3.1 Servo-actuator system dynamics

3.1.1 Block diagram

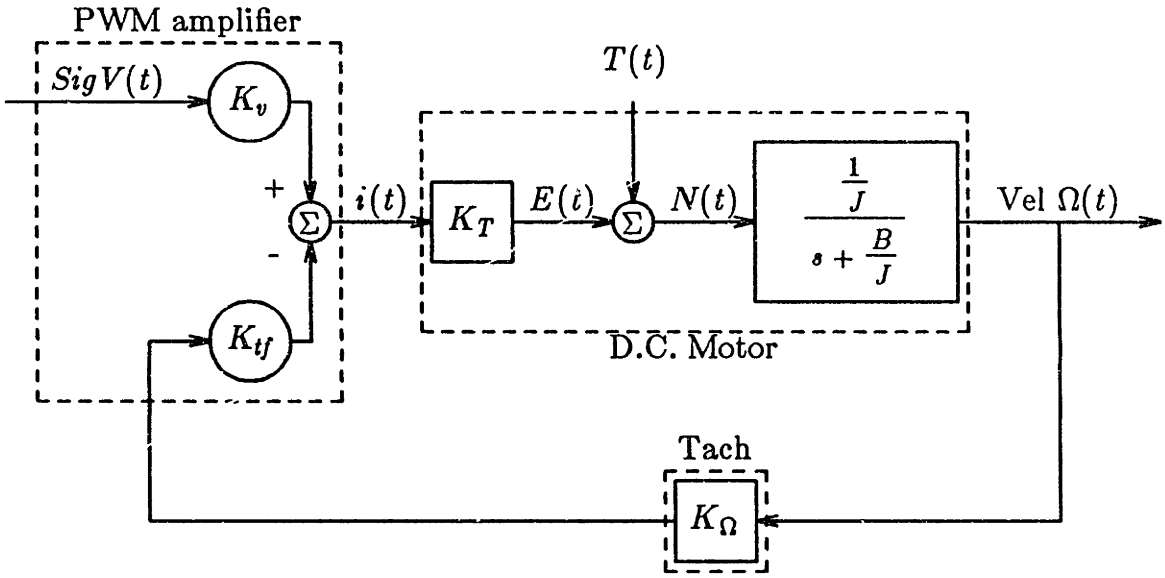

Figure 3.2. Block diagram of servo-actuator system

3.1.2 Parameters

K_v = signal gain (pot adjustable) *amps/volt*

K_{tf} = tach feedback gain (pot adjustable) *amps/volt*

K_Ω = tach constant = $\frac{7\ volts}{1000\ rpm} = \frac{0.067\ volts}{rad/sec}$

K_T = torque constant = *38.5 oz-in/amp*

J = motor-tach inertia (*oz-in-sec* ^{2})

B = motor-tach viscous damping *(oz-in-sec)*

3.1.3 Model

In the continuous time domain the actuator (master and slave actuators are structurally identical) dynamics can be represented by

$$J \frac{d}{dt}\Omega(t) + B\,\Omega(t) = T(t) + E(t) \tag{3.1}$$

where $T(t)$ is the external torque imposed on the motor shaft, and $E(t)$ is the electro-magnetic torque imposed by the motor armature on the motor rotor.

A tachometer feedback loop in the PWM servo-amplifer is used to adjust the bandwidth of the servo-actuator to a desired value. This feedback loop is distinct from the velocity feedback used to determine the structure of the impedance matrix in the preceding chapter, and is analog in nature.

From the block diagram

$$\begin{aligned} E(t) = K_T\, i(t) &= K_T(K_v V(t) - K_{tf} K_\Omega \Omega(t)) \\ &= U(t) - K_T K_{tf} K_\Omega \Omega(t) \end{aligned} \tag{3.2}$$

where

$$U(t) = \textit{ control torque } = K_T K_v V(t) \tag{3.3}$$

Therefore

$$J \frac{d}{dt}\Omega(t) + (B + K_T K_{tf} K_\omega)\,\Omega(t) = T(t) + U(t) \tag{3.4}$$

or

$$\frac{d}{dt}\Omega(t) = -\frac{B + K_T K_{tf} K_\omega}{J}\,\Omega(t) + \frac{1}{J}\,(T(t) + U(t))$$

$$= -a\,\Omega(t) + b\,(T(t) + U(t)) \tag{3.5}$$

$$a = \frac{B + K_T K_{tf} K_\Omega}{J} \qquad and \qquad b = \frac{1}{J}$$

Therefore the transfer function to output velocity (Ω) from input torque (net torque $N(t)$=$T(t)$+$U(t)$) is

$$\frac{\Omega(s)}{N(s)} = \frac{b}{s+a} = \frac{b}{a}\,\frac{a}{s+a} \tag{3.6}$$

Using the subscripts m and s for master and slave actuator parameters and variables, the master and slave servo-actuator impedances (see Fig. 2.6) are

$$Z_{ma}(s) = \frac{1}{b_m}s + \frac{a_m}{b_m} \tag{3.7}$$

$$Z_{sa}(s) = \frac{1}{b_s}s + \frac{a_s}{b_s} \tag{3.8}$$

3.2 Servo-actuator bandwidth adjustment

As mentioned previously, an internal velocity feedback loop is used to set the bandwidth of the servo-actuator. The tach feedback gain K_{tf} will be selected to set the time constant for the actuator to be 0.1 secs.

The transfer function from the control signal (V in volts) to the angular velocity (Ω in rad/sec) is given by

$$\frac{\Omega(s)}{V(s)} = K_v \frac{\frac{K_T}{J}}{s+\frac{B}{J}+\frac{K_T K_\Omega K_{tf}}{J}} \tag{3.9}$$

The open loop time constant and steady-state gain are

$$\tau_{ol} = \frac{J}{B} \tag{3.10}$$

$$\frac{\Omega_{ss}}{V_{ss}} = \frac{K_v K_T}{B} \tag{3.11}$$

The measured† open loop steady-state gain is $\approx 100 \frac{rad/sec}{volt}$. Hence the damping $B = .385$ *oz-in-sec* ($K_v = 1$ *amp/volt*). The measured open loop time constant is *0.7 secs*, hence $J = 0.27$ *oz-in-sec*^{2}.

The time constant with the velocity feedback is

$$\tau = \frac{J}{B+K_T K_\Omega K_{tf}} \tag{3.12}$$

$$\textit{hence}\quad K_{tf} = \left(\frac{J}{\tau} - B\right)\frac{1}{K_\Omega K_T} = 0.9 \textit{ amps/volt} \qquad \textit{for } \tau = 0.1 \textit{ sec}$$

With $K_v = 1$ *amp/volt* (this maps the $\pm$ 10 V range of the D/A outputs to a $\pm$ 10

† The viscous damping is a non-linear function of the magnitude and sense of angular velocity, so the steady-state gain reported is an average value over a range of angular velocities.

amps command to the PWM amplifier) and $K_{tf} = 0.9$ *amps/volt*, at steady state conditions

$$\frac{\Omega_{ss}}{V_{ss}} = \frac{K_T K_v}{B + K_T K_\Omega K_{tf}} = 14.2 \frac{rad/sec}{volt}$$

The transfer function is then

$$\frac{\Omega(s)}{V(s)} = \frac{14.2}{0.1s + 1} \tag{3.13}$$

3.2.1 Calibration procedure

1. Set input control signal $V = 0.0$ volts and adjust balance pot till ammeter in series with motor reads 0 amps.

2. Clamp motor shaft, set input control signal $V = 5$ volts and adjust signal gain potentiometer (K_v) till ammeter reads 5 amps. Check that ammeter reads -5 amps for a -5 volt input and adjust balance if necessary. This sets $K_v = 1$.

3. Unclamp motor shaft, set V = 5 volts and adjust the tach pot (K_{tf}) till the tach output voltage = 5 x 14.2 x 0.067 = 4.76 volts. This sets $K_{tf} =$ 0.9 and consequently $\tau = 0.1$.

4. Sampled Data Model of Master-Slave Manipulator

There are two approaches to developing a sampled data model for the MSM. One method is to start with the continuous time differential equations that describe the dynamics of the system, and solve for the state of the system at the sampling instants. This solution takes the form of a difference equation that describes the evolution of the system state at discrete time intervals. A z-transform applied to the difference equations yields the network function for the system in the z-domain.

An alternative method is to map the system network function in the the s-domain to the z-domain by one of many approximations that are commonly used.

It is convenient to keep the design process in the continuous time domain so that many useful theorems and design tools from a vast body of literature can be applied. One of the goals in developing the sampled-data model of the MSM is to relate the results from the design process in the s-domain to design parameters in the z-domain. More specifically, the relationship between the feedback gain matrix $[K]$ in the s-domain and the corresponding gain matrix $[H]$ in the z-domain is of interest.

To keep notation simple, we shall generally use the same symbols for s-domain and z-domain variables, indicating which one we mean by the argument s or z. The z-domain open-circuit impedances, for example, will thus be denoted by

$Z_{ij}(z)$. This is common but convenient "abuse of notation".

The procedure adopted here to find this relationship is as follows:

1. Find the open-circuit impedance parameters $Z_{ij}(z)$ in the z-domain, by taking the z-transform of the difference equations that result from the first approach outlined previously. These parameters are functions of a gain matrix $[H]$.

2. Map the open-circuit impedance parameters in the s-domain, i.e. $Z_{ij}(s)$, into the z-domain by applying a Zero-Order-Hold (ZOH) equivalent transformation. These resulting parameters in the z-domain are functions of the gain matrix $[K]$.

3. Equate $Z_{ij}(z)$ obtained from the two routes outlined above to solve for the elements of $[H]$ in terms of the elements of $[K]$.

This chapter demonstrates these steps.

4.1 Sampled data model of the servo-actuator

In the continuous time domain, the master actuator dynamics (3.5) is represented by

$$\frac{d}{dt}\Omega_m(t) = -a_m\Omega_m(t) + b_m(T_m(t) + U_m(t)) \tag{4.1}$$

$$a_m = \frac{B_m + K_T K_t K_\Omega}{J_m} \qquad and \qquad b_m = \frac{1}{J_m}$$

The solution for this first order differential equation is

$$\Omega_m(t) = \Omega_m(t_0) e^{-a_m(t-t_0)} + \int_{t_0}^{t} b_m e^{-a_m(t-\tau)} (T_m(\tau) + U_m(\tau)) d\tau \qquad (4.2)$$

Suppose the system is sampled at discrete time intervals of T, i.e., the sampling frequency is f_s ($= \frac{1}{T}$). Then the evolution of the state of the sampled system from one sampling instant to the next (i.e. from $t_i = t_0 + iT$, the ith sampling instant, to $t_{i+1} = t_i + T$, the next sampling instant) can be written as

$$\Omega_m(t_{i+1}) = \Omega_m(t_i) e^{-a_m(T)} + \int_{t_i}^{t_i+T} b_m e^{-a_m(iT+T-\tau)} (T_m(\tau) + U_m(\tau)) d\tau \qquad (4.3)$$

The control torque $U_m(t)$ is a piecewise constant function, since the control signal (V_m) is the output from a Digital to Analog converter, i.e.,

$$U_m(t) = U_m(iT) \quad for \quad t_i < t < t_{i+1} \qquad (4.4)$$

and hence can be taken out of the integral in (4.3). However the external torque $T_m(t)$ is a continuous time function which is not sampled. A simplifying assumption that is made here is that $T_m(t)$ is also piecewise constant. Such an assumption can be justified if the bandwidth of the external torque signal is much lower than the sampling frequency. Since this torque is applied by the human operator at the master port of the MSM, its bandwidth is normally of the order of 1 Hz, which is much lower than the sampling frequency of 60 Hz. If the torque from the environment at the slave port is also limited to a bandwidth of 10 Hz or less, both external torques can be considered to be constant within the sampling interval.

Hence the torque applied by the human operator at the master port may be represented as

$$T_m(t) = T_m(iT) \quad for \quad t_i < t < t_{i+1} \tag{4.5}$$

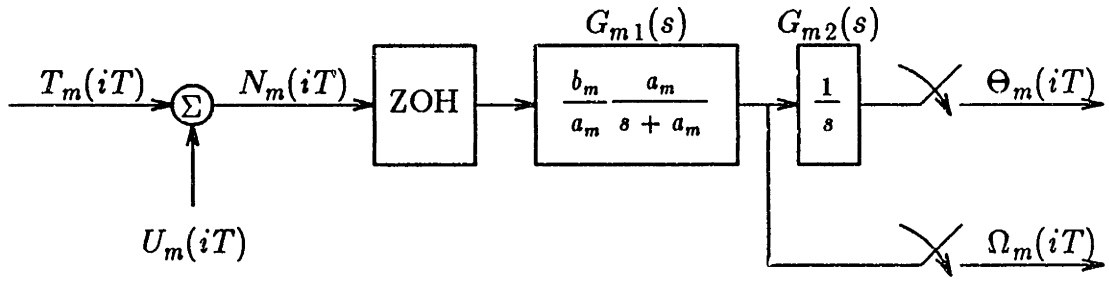

Figure 4.1. Block diagram of sampled data model of servo-actuator.

Then the dynamics of the sampled data system can be simplified to be

$$\Omega_m(iT+T) = e^{-a_m T}\Omega_m(iT) + b_m(T_m(iT) + U_m(iT)) \int_{iT}^{iT+T} e^{-a_m(iT+T-\tau)} d\tau$$

On substituting $\eta = iT+T-\tau$,

$$\begin{aligned}\Omega_m(iT+T) &= e^{-a_m T}\Omega_m(iT) + b_m(T_m(iT) + U_m(iT)) \int_{\eta=0}^{\eta=T} e^{-a_m\eta} d\eta \\ &= e^{-a_m T}\Omega_m(iT) + \frac{b_m}{a_m}(1-e^{-a_m T})(T_m(iT) + U_m(iT)) \end{aligned} \tag{4.6}$$

Assuming zero initial conditions and applying the z-transform to (4.6) the z-domain transfer function is

$$z\Omega_m(z) = e^{-a_m T}\Omega_m(z) + \frac{b_m}{a_m}(1-e^{-a_m T})(T_m(z) + U_m(z))$$

or

$$\frac{a_m}{b_m}\frac{(z-e^{-a_m T})}{(1-e^{-a_m T})}\Omega_m(z) = T_m(z) + U_m(z) \tag{4.7}$$

This yields the following servo-actuator impedance in the z-domain

$$Z_{ma}(z) = \frac{a_m}{b_m} \frac{(z - e^{-a_m T})}{(1 - e^{-a_m T})} \tag{4.8}$$

Since the slave servo-actuator is structurally similar, we get

$$Z_{sa}(z) = \frac{a_s}{b_s} \frac{(z - e^{-a_s T})}{(1 - e^{-a_s T})} \tag{4.9}$$

Once again, the control signals that form the dependent sources are chosen to be linear nondynamic functions of the master and slave actuator state variables:

$$\begin{Bmatrix} U_m(iT) \\ U_s(iT) \end{Bmatrix} = \begin{bmatrix} -h_{11} & -h_{12} & h_{13} & h_{14} \\ h_{21} & h_{22} & -h_{23} & -h_{24} \end{bmatrix} \begin{Bmatrix} \Theta_m(iT) \\ \Omega_m(iT) \\ \Theta_s(iT) \\ \Omega_s(iT) \end{Bmatrix} \tag{4.10}$$

where h_{ij} are elements of the 2 x 4 feedback gain matrix $[H]$.

The subsequent z-transform yields

$$\begin{Bmatrix} U_m(z) \\ U_s(z) \end{Bmatrix} = \begin{bmatrix} -h_{11} & -h_{12} & h_{13} & h_{14} \\ h_{21} & h_{22} & -h_{23} & -h_{24} \end{bmatrix} \begin{Bmatrix} \Theta_m(z) \\ \Omega_m(z) \\ \Theta_s(z) \\ \Omega_s(z) \end{Bmatrix} \tag{4.11}$$

In order to obtain a z-domain transfer function between the sampled velocity vector and the sampled torque vector, the sampled position vector has to be eliminated from (4.11). In the s-domain case the relationship $\Omega_m(s) = s\Theta_m(s)$ allowed this. To find an analogous relationship between $\Theta_m(z)$ and $\Omega_m(z)$, the transfer

functions between the net torque $N_m(z)$ $(=T_m(z)+U_m(z))$ and the position and velocity, represented by $G_m(z)$ and $G_{m1}(z)$ respectively in Fig. 4.2, are first determined.

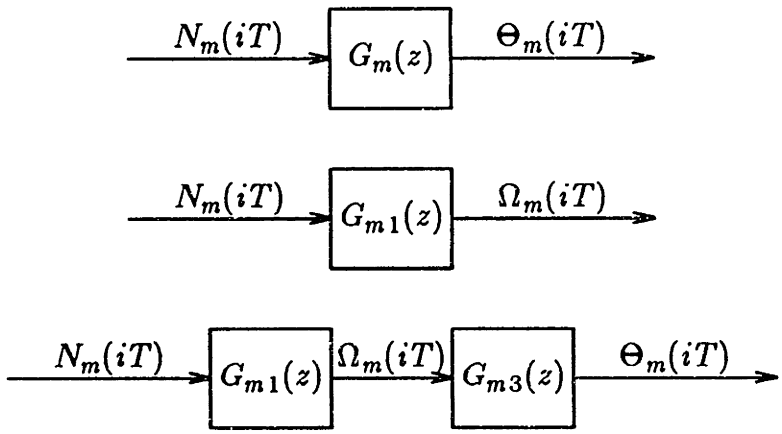

Figure 4.2. Transfer function from sampled velocity to sampled position.

The ZOH equivalent of $G_m(s)(=G_{m1}(s)G_{m2}(s))$ can be shown to be

$$G_m(z) = \frac{\Theta_m(z)}{N_m(z)} = \frac{b_m}{a_m} \frac{(a_m T - 1 + e^{-a_m T})z + (1 - e^{-a_m T} - a_m T e^{-a_m T})}{a_m (z-1)(z - e^{-a_m T})} \tag{4.12}$$

and the ZOH equivalent of $G_{m1}(s)$ from (3.7) is

$$G_{m1}(z) = \frac{\Omega_m(z)}{N_m(z)} = \frac{b_m}{a_m} \frac{1 - e^{-a_m T}}{z - e^{-a_m T}} \tag{4.13}$$

Hence

$$G_{m3}(z) = \frac{G_m(z)}{G_{m1}(z)} = \frac{\Theta_m(z)}{\Omega_m(z)} = \frac{(a_m T - 1 + e^{-a_m T})z + (1 - e^{-a_m T} - a_m T e^{-a_m T})}{a_m (z-1)(1 - e^{-a_m T})}$$

$$= d_m \left\{ \frac{z+c_m}{z-1} \right\} \tag{4.14}$$

where

$$c_m = \frac{1-e^{-a_m T}-a_m T e^{-a_m T}}{a_m T-1+e^{-a_m T}} \tag{4.15}$$

$$d_m = \frac{a_m T-1+e^{-a_m T}}{a_m(1-e^{-a_m T})} \tag{4.16}$$

Note that

$$d_m(c_m + 1) = T \tag{4.17}$$

The transfer function between the sampled position and the sampled velocity is therefore given by

$$\Theta_m(z) = d_m \frac{z+c_m}{z-1} \Omega_m(z) \tag{4.18}$$

Substituting for $\Theta_m(z)$ and $\Theta_s(z)$ in (4.11) yields

$$\begin{Bmatrix} U_m(z) \\ U_s(z) \end{Bmatrix} = \begin{bmatrix} -\left(h_{11} d_m \frac{z+c_m}{z-1} + h_{12}\right) & h_{13} d_s \frac{z+c_s}{z-1} + h_{14} \\ h_{21} d_m \frac{z+c_m}{z-1} + h_{22} & -\left(h_{23} d_s \frac{z+c_s}{z-1} + h_{24}\right) \end{bmatrix} \begin{Bmatrix} \Omega_m(z) \\ \Omega_s(z) \end{Bmatrix} \tag{4.19}$$

Thus

$$f_{11}(z) = h_{11} d_m \frac{z+c_m}{z-1} + h_{12}$$

$$f_{12}(z) = h_{13} d_s \frac{z+c_s}{z-1} + h_{14}$$

$$f_{21}(z) = h_{21}\, d_m \frac{z+c_m}{z-1} + h_{22}$$

$$f_{22}(z) = h_{23}\, d_s \frac{z+c_s}{z-1} + h_{24}$$

Since

$$T_m(z) = Z_{ma}(z)\, \Omega_m(z) - U_m(z)$$

and

$$T_s(z) = Z_{sa}(z)\, \Omega_s(z) - U_s(z)$$

substituting for the dependent sources $U_m(z)$ and $U_s(z)$ yields the z-domain representation of the impedance matrix for the MSM :

$$\begin{Bmatrix} T_m(z) \\ T_s(z) \end{Bmatrix} = \begin{bmatrix} Z_{ma}(z) + f_{11}(z) & -f_{12}(z) \\ -f_{21}(z) & Z_{sa}(z) + f_{22}(z) \end{bmatrix} \begin{Bmatrix} \Omega_m(z) \\ \Omega_s(z) \end{Bmatrix} \tag{4.20}$$

The components of the impedance matrix are

$$Z_{11}(z) = \frac{a_m}{b_m} \frac{z-e^{-a_m T}}{1-e^{-a_m T}} + h_{11}\, d_m \frac{z+c_m}{z-1} + h_{12} \tag{4.21}$$

$$Z_{12}(z) = -\left(h_{13}\, d_s \frac{z+c_s}{z-1} + h_{14} \right) \tag{4.22}$$

$$Z_{21}(z) = -\left(h_{21}\, d_m \frac{z+c_m}{z-1} + h_{22} \right) \tag{4.23}$$

$$Z_{22}(z) = \frac{a_s}{b_s} \frac{z-e^{-a_s T}}{1-e^{-a_s T}} + h_{23}\, d_s \frac{z+c_s}{z-1} + h_{24} \tag{4.24}$$

This completes the first step in the process. The next step is to find the ZOH equivalents of the $Z_{ij}(s)$. As an example, consider $Z_{12}(s)$:

$$-Z_{12}(s) = k_{14} + \frac{k_{13}}{s}$$

The ZOH equivalent of $Z_{12}(s)$ is

$$\begin{aligned} &\frac{z-1}{z}\mathbf{Z}\left\{\left(\frac{k_{14}}{s} + \frac{k_{13}}{s^2}\right)\right\} \\ &= \frac{z-1}{z}\left\{k_{14}\frac{z}{z-1} + k_{13}\frac{T\,z}{(z-1)^2}\right\} \\ &= \frac{z\,(k_{14}) + (k_{13}T - k_{14})}{z-1} \end{aligned} \tag{4.25}$$

where $\mathbf{Z}$ represents the z-transform.

The final step is to equate the above with the form obtained in the first step.

From (4.22)

$$-Z_{12}(z) = \frac{z\,(h_{13}d_s + h_{14}) + (h_{13}d_s c_s - h_{14})}{z-1} \tag{4.26}$$

On equating coefficients with (4.26) :

$$h_{13}d_s + h_{14} = k_{14}$$

and

$$h_{13}d_s c_s - h_{14} = k_{13}T - k_{14}$$

These two simultaneous equations yield the sampled data system feedback gains in terms of the continuous time system feedback gains

$$h_{13} = \frac{k_{13}\,T}{d_s(c_s+1)} = k_{13} \tag{4.27}$$

$$h_{14} = k_{14} - h_{13}\,d_s = k_{14} - k_{13}\,d_s \tag{4.28}$$

In applying this process to the diagonal elements of $[Z(s)]$, namely $Z_{11}(s)$ and $Z_{22}(s)$, one additional approximation has to be introduced.

$$Z_{11}(s) = \frac{1}{b_m}s + \frac{a_m}{b_m} + k_{12} + \frac{k_{11}}{s}$$

Since the first term in the impedance function is a differentiator, it is not possible to find a ZOH equivalent for it, and some other form of approximation has to be used. ZOH equivalents for the remaining terms can be evaluated as in the previous case. Using a forward rectangular rule to approximate the differentiator yields

$$ZOH\left\{Z_{11}(s)\right\} = \frac{1}{b_m}\frac{z-1}{T} + ZOH\left\{\frac{a_m}{b_m} + k_{12} + \frac{k_{11}}{s}\right\} \tag{4.29}$$

$$= \frac{1}{b_m}\frac{z-1}{T} + \frac{a_m}{b_m} + k_{12} + k_{11}\frac{T}{z-1}$$

$$= \frac{\dfrac{1}{b_m T}\,z^2 + \left[\dfrac{a_m T - 2}{b_m T} + k_{12}\right]z + \left[\dfrac{1 - a_m T}{b_m T} + k_{11}T - k_{12}\right]}{z-1}$$

From (4.21) and approximating $e^{-a_m T}$ by $(1 - a_m T)$

$$Z_{11}(z) = \frac{\dfrac{1}{b_m T}\,z^2 + \left[\dfrac{a_m T - 2}{b_m T} + h_{11}d_m + h_{12}\right]z + \left[\dfrac{1 - a_m T}{b_m T} + h_{11}d_m c_m - h_{12}\right]}{z-1}$$

Equating coefficients of z

$$h_{11} d_m + h_{12} = k_{12}$$

and

$$h_{11} d_m c_m - h_{12} = k_{11} T - k_{12}$$

Solving for h_{11} and h_{12}, we get

$$h_{11} = \frac{k_{11} T}{d_m(c_m + 1)} = k_{11} \tag{4.30}$$

$$h_{12} = k_{12} - k_{11}\ d_m \tag{4.31}$$

The equations (4.27), (4.28), (4.30) and (4.31) establish the relationship between the position and velocity gains in the continuous and sampled data systems. Hence by analogy the remaining gains for the discrete case are

$$h_{21} = k_{21} \tag{4.32}$$

$$h_{22} = k_{22} - k_{21}\ d_m \tag{4.33}$$

$$h_{23} = k_{23} \tag{4.34}$$

$$h_{24} = k_{24} - k_{23}\ d_s \tag{4.35}$$

This completes the process for relating the continuous time feedback gain matrix $[K]$ to its counterpart in the discrete time case $[H]$.

5. Design Goals: Stability and Desired Port Impedances

The model for the MSM that has been developed to this point includes two dependent sources, $U_m(s)$ at the master port and $U_s(s)$ at the slave port, that are functions of the flow and effort variables at the two ports. The gain matrix $[K]$ that relates the dependent sources to the port variables will be selected to meet two goals:

1. The 2-port MSM has to be stable for any passive termination $Z_h(s)$ at the master port, and any passive termination $Z_t(s)$ at the slave port.

2. The port impedances, $Z_m(s)$ at the master port and $Z_s(s)$ at the slave port, have to match desired values specified by the designer.

By stability we mean that the reponse at either port to a bounded excitation (at either port) or to non-zero initial conditions is bounded. This requirement is realized in the frequency domain by the location of all poles of the appropriate network functions in the open left half plane of the s-domain (LHS) for "strict stability" and the closed LHS for "simple stability". The approach to realizing this stability goal is presented in this chapter.

Though we chose to model both the human and task impedances, $Z_h(s)$ and $Z_t(s)$ as second order network functions in Chapter 2, in condition (1) we are far more conservative by designing for stability for any passive $Z_h(s)$ and $Z_t(s)$. We

are therefore covered for more complicated models of the human and task impedances. If more information on these impedances were available, e.g. bounds on parameter variations, then the design can afford to be less conservative.

As will be shown at a later point in this chapter, the port impedances $Z_m(s)$ and $Z_s(s)$ are rational functions with 4th order numerator polynomials and 3rd order denominator polynomials. Since the response is dominated by the "stiffness" component of the impedances at low frequencies, the desired stiffnesses at the ports K_m and K_s will be the specified as the design parameters, rather than attempting to specify desired rationals in s for the impedances.

By combining the conditions for stability and the conditions to realize desired port stiffnesses, the constraints on selection of $[K]$ are derived and used in the design process.

5.1 Stability analysis

5.1.1 An initial approach

We start the stability analysis by recognizing that the MSM is potentially unstable due to the presence of the feedback to the dependent torque sources. A reasonable initial approach to stabilizing the active 2-port MSM network is to look at the master port impedance $Z_m(s)$ when the slave port is terminated by a passive task impedance $Z_t(s)$. The response at the master port is determined by

$Z_m(s)$ in series with $Z_h(s)$.

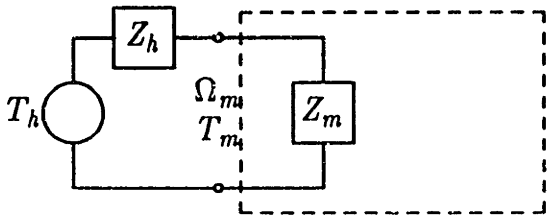

Figure 5.1. Master port termination.

Since (2.25) shows that

$$Z_m(s) = Z_{11}(s) - \frac{Z_{12}(s)Z_{21}(s)}{Z_{22}(s) + Z_t(s)}$$

Substituting the rational functions that represent the open-circuit impedance parameters $Z_{ij}(s)$ (see (2.17), (2.18), (2.19), (2.19) and (2.28), (2.29), (2.30), (2.31)), yields

$$Z_m(s) = \frac{T_m(s)}{\Omega_m(s)} = \frac{1}{s}\frac{\prod_{i=1}^{4}(s-z_{mi})}{\prod_{j=1}^{2}(s-p_{mj})}$$

$$= \frac{1}{s}\frac{a_{4m}s^4+a_{3m}s^3+a_{2m}s^2+a_{1m}s+a_{0m}}{b_{2m}s^2+b_{1m}s+b_{0m}} \tag{5.1}$$

where

$$a_{4m} = (\frac{1}{b_s}+J_t)\frac{1}{b_m}$$

$$a_{3m} = (\frac{1}{b_s}+J_t)(\frac{a_m}{b_m}+k_{12}) + (\frac{a_s}{b_s}+k_{24}+B_t)\frac{1}{b_m}$$

$$a_{2m} = k_{11}(\frac{1}{b_s}+J_t) + (\frac{a_s}{b_s}+k_{24}+B_t)(\frac{a_m}{b_m}+k_{12}) + (k_{23}+K_t)\frac{1}{b_m} - k_{14}k_{22}$$

$$a_{1m} = k_{11}(\frac{a_s}{b_s}+k_{24}+B_t) + (\frac{a_m}{b_m}+k_{12})(k_{23}+K_t) - k_{14}k_{21} - k_{13}k_{22}$$

$$a_{0m} = k_{11}(k_{23}+K_t) - k_{13}k_{21}$$

$$b_{2m} = (\frac{1}{b_s}+J_t)$$

$$b_{1m} = (\frac{a_s}{b_s}+k_{24}+B_t)$$

$$b_{0m} = (k_{23}+K_t)$$

Since $Z_m(s)$ is a driving point impedance, the system in Fig. 5.1 will be stable only if $Z_m(s)$ has no poles or zeros in the RHS. This necessary condition follows from the requirement for stability in two special cases, $Z_h(s) = \infty$ (open circuit) and $Z_h(s) = 0$ (short circuit) respectively. By applying the Routh-Hurwitz stability criterion to both numerator and denominator polynomials in (5.1), corresponding constraints on the gains k_{ij} to obtain such a stable, minimum phase $Z_m(s)$ can be derived.

For the denominator polynomial, all the coefficients must have the same sign:

$$b_{2m} > 0 \quad since \quad J_t > 0 \quad and \quad b_s > 0$$

$$b_{1m} > 0 \quad implies \quad k_{24} > -\frac{a_s}{b_s}$$

$$b_{0m} > 0 \quad implies \quad k_{23} > -K_t$$

For the numerator polynomial the Routh-Hurwitz array is

$$
\begin{array}{c|c|c}
a_{4m} & a_{2m} & a_{0m} \\
a_{3m} & a_{1m} & \\
b_1 = \dfrac{a_{3m}a_{2m} - a_{1m}a_{4m}}{a_{3m}} & b_2 = a_{0m} & \\
c_1 = \dfrac{b_{1m}a_{1m} - a_{3m}a_{0m}}{b_{1m}} & & \\
a_{0m} & &
\end{array}
$$

All the members of the first column must have the same sign. Since a_{4m} is known to be positive, all the other members of the first column must also be positive.

$$
a_{3m} > 0 \quad \textit{implies} \quad k_{24} > -\frac{a_s}{b_s} \quad \textit{and} \quad k_{12} > -\frac{a_m}{b_m}
$$

$$
a_{0m} > 0 \quad \textit{implies} \quad k_{23}k_{11} > {k_{13}}^2
$$

$$
b_1 > 0 \quad \textit{implies} \quad (a_{3m}a_{2m} - a_{1m}a_{4m}) > 0
$$

$$
c_1 > 0 \quad \textit{implies} \quad (b_1 a_{1m} - a_{3m}a_{0m}) > 0
$$

There are three problems with this approach:

1. The stability constraints are dependent on the values of the task impedance parameter K_t. This can be overcome by modifying the constraint that $k_{23} > -K_t$ to be the more conservative constraint $k_{23} > 0$ since K_t is always > 0. If more refined bounds on K_t are available, these could be used instead.

2. Two of the constraints, $b_1 > 0$ and $c_1 > 0$ yield complicated equations to be solved for values of the gains k_{ij}.

3. The most serious problem with this approach is that making $Z_m(s)$ stable and minimum phase does not ensure that the 2-port will be stable for

passive terminations $Z_h(s)$ other than 0 or ∞ at the master port. To achieve this, the numerator of the network function $Z_h(s) + Z_m(s)$ for all passive $Z_h(s)$ has to have roots in the LHS, since this numerator (before any order reduction due to cancellations) is the characteristic polynomial of the system in Fig. 5.1.

5.1.2 Using positive real functions

A second approach to stabilizing the active 2-port MSM uses the concept of positive real (PR) functions from electrical network theory. A passive multiport network (which is inherently stable) has the characterizing property that its impedance and admittance matrices are PR[36]. We begin with the definition of PR for the case of scalar functions.

A function $F(s)$ of a complex variable s $(=\sigma+j\omega)$ is said to be positive-real if it satisfies three conditions[37] [38] [39]:

1. $F(s)$ is analytic in the open RHS,
2. $F(\sigma)$ is real,
3. $\mathrm{Re}[F(s)] \geq 0$ for $\mathrm{Re}[s] \geq 0$

It can be shown that[37] the first condition is redundant for rational functions (which are what we are interested in), since the other two conditions will require that $F(s)$ be devoid of poles in the open RHS. The second condition is

always satisfied for a real rational function since all the coefficients of the numerator and denominator polynomials of such a function are real. Therefore a real rational function is PR if and only if:

1. $\mathrm{Re}[F(s)] \geq 0$ for $\mathrm{Re}[s] \geq 0$

A set of equivalent conditions[36] (for positive realness of a real rational function) that is usually much simpler to apply is the following:

1. $F(s)$ has no poles in the open RHS,
2. Poles on the $j\omega$-axis, if they exist, are simple, and residues evaluated at these poles are real and postive.
3. $Re[F(j\omega)] \geq 0$ for all ω, except at any poles on the $j\omega$ axis.

Note that the second condition requires that the degree of the denominator differ from that of the numerator by no more than 1.

Properties of PR functions[36] that are relevant in this context are:

1. If $F_1(s)$ is PR and $F_2(s)$ is PR, $F_1(s) + F_2(s)$ is also PR.
2. If $F(s)$ is PR, so are $\frac{1}{F(s)}$ and $F(\frac{1}{s})$.
3. As a consequence of the above, a PR function has no poles or zeros in the open RHS.

Using the above facts, it becomes evident that one way to make the MSM stable is to ensure that $Z_m(s)$ is PR; since the passive $Z_h(s)$ is PR, the network function

$Z_m(s) + Z_h(s)$ is PR and hence the system is stable.

The problem, however is to ensure that $Z_m(s)$ is PR for all passive task impedances $Z_t(s)$. We shall see how far reasoning based on scalar PR functions leads us, before turning to PR matrices for a satisfactory resolution of the stability problem.

It can be shown[36][40] that one of the three conditions above for $Z_m(s)$ to be PR, namely the condition $\mathrm{Re}[Z_m(j\omega)] \geq 0$ for all ω except at the poles, is equivalent to the condition

$$\mathrm{Re}[Z_{11}(j\omega)] \cdot \mathrm{Re}[Z_{22}(j\omega)] \geq \frac{1}{2} \mid Z_{12}(j\omega)\, Z_{21}(j\omega) \mid (1+\cos\theta) \tag{5.2}$$

at all such ω, provided

$$\mathrm{Re}[Z_{11}(j\omega)] > 0 \tag{5.3}$$

where

$$\theta = \tan^{-1} \frac{\mathrm{Im}[Z_{12}(j\omega)\, Z_{21}(j\omega)]}{\mathrm{Re}[Z_{12}(j\omega)\, Z_{21}(j\omega)]} \tag{5.4}$$

The condition above is part of what is referred to as Llewellyn's stability criterion for 2-port networks. Note that (5.2) does not involve $Z_t(s)$, and also that it implies

$$\mathrm{Re}[Z_{22}(j\omega)] \geq 0 \tag{5.5}$$

A special case is the *reciprocal* 2-port network, $Z_{12}(s) = Z_{21}(s)$, which yields the simpler condition

$$\mathrm{Re}[Z_{11}(j\omega)]\,\mathrm{Re}[Z_{22}(j\omega)] \geq (\mathrm{Re}[Z_{12}(j\omega)])^2 \tag{5.6}$$

The special reciprocal case condition is part of what is referred to as the Gewertz stability condition.

At frequencies where $\mathrm{Re}[Z_{11}(j\omega)] = 0$, the development in [36][40] can be used to show that the condition

$$\mathrm{Re}[Z_{22}(j\omega)] \geq -\mathrm{Re}[Z_t(j\omega)] \tag{5.7}$$

is equivalent to $\mathrm{Re}[Z_m(j\omega)] \geq 0$ in the reciprocal case. This condition depends on the task impedance $Z_t(s)$, however.

Substituting for $Z_{ij}(j\omega)$ yields

$$\mathrm{Re}[Z_{11}(j\omega)] = \frac{a_m}{b_m} + k_{12}$$

$$\mathrm{Re}[Z_{22}(j\omega)] = \frac{a_s}{b_s} + k_{24}$$

$$\mathrm{Re}[Z_{12}(j\omega)] = k_{14}$$

$$\mathrm{Re}[Z_{21}(j\omega)] = k_{21}$$

If the MSM is constrained to be *reciprocal*, so $k_{14} = k_{21}$, then the above conditions become

$$k_{12} \geq -\frac{a_m}{b_m} \tag{5.8}$$

$$k_{24} \geq -\frac{a_s}{b_s} \tag{5.9}$$

$$k_{14} \leq \left[\left(\frac{a_m}{b_m} + k_{12}\right)\left(\frac{a_s}{b_s} + k_{24}\right)\right]^{1/2} \tag{5.10}$$

These conditions provide constraints on four of the eight elements of the feedback gain matrix.

On recalling the conditions for $Z_m(s)$ to be PR, however it is apparent that Llewellyn's (and Gewertz's) conditions are necessary but not sufficient. Since $Z_m(s)$ has a simple pole on the jw-axis, its residue at that pole has to be real and positive, and, $Z_m(s)$ has to be shown to be analytic in the RHS. Neither of these two conditions is guaranteed by Llewellyn's conditions alone.

The conditions for analyticity in the RHS have already been discussed in section 5.1.1, but are unfortunately dependent on the task impedance. The residue of $Z_m(s)$ a the pole $s=0$ is seen from (5.1) to be a_{0m}/b_{0m}. Since analyticity requires $b_{0m}>0$, we see that the condition on the residue requires

$$a_{0m} = k_{11}(k_{23} + K_t) - k_{13}\ k_{21} > 0 \tag{5.11}$$

This condition again depends on knowledge of $Z_t(s)$, unfortunately.

5.1.3 Using positive real matrices

A third and more general approach for a n-port network is to require that the immitance matrix for the n-port network be positive real. This is equivalent to constraining the n-port described by the matrix $[Z(s)]$ or $[Y(s)]$ to be passive, and hence inherently stable.

The criteria that have to be satisfied by the impedance matrix are

1. $Z_{ij}(\sigma)$ is real.

2. $Z_{ij}(s)$ is analytic in the RHS.

3. Poles of $Z_{ij}(j\omega)$ are simple, and the hermitian residue matrix at each of these poles is positive-semidefinite.

4. The determinant of the hermitian matrix of the impedance function is non-negative for all ω.

Equivalently similar conditions have to be satisfied by $Y(s)$.

Conditions (1) and (2) are satisfied by $Z_{ij}(s)$.

The hermitian residue matrix for the simple pole on the $j\omega$ axis, namely the one at $s=0$, is

$$\begin{bmatrix} k_{11} & -k_{13} \\ -k_{13} & k_{23} \end{bmatrix}$$

Applying (3) yields:

$$k_{11} \geq 0 \tag{5.12}$$

$$k_{23} \geq 0 \tag{5.13}$$

$$k_{11}k_{23} \geq {k_{13}}^2 \tag{5.14}$$

The hermitian matrix of $[Z(s)]$ on the $j\omega$ axis, for the reciprocal case, is given by:

$$\begin{bmatrix} \mathrm{Re}[Z_{11}(j\omega)] & \mathrm{Re}[Z_{12}(j\omega)] \\ \mathrm{Re}[Z_{12}(j\omega)] & \mathrm{Re}[Z_{22}(j\omega)] \end{bmatrix}$$

Applying (4) yields:

$$\mathrm{Re}[Z_{11}(j\omega)] \geq 0 \quad i.e. \quad k_{12} \geq -\frac{a_m}{b_m} \tag{5.15}$$

$$\mathrm{Re}[Z_{22}(j\omega)] \geq 0 \quad i.e. \quad k_{24} \geq -\frac{a_s}{b_s} \tag{5.16}$$

$$\mathrm{Re}[Z_{11}(j\omega)]\cdot\mathrm{Re}[Z_{22}(j\omega)] \geq (\mathrm{Re}[Z_{12}(j\omega)])^2$$

$$i.e. \quad k_{14} \leq \left[(\frac{a_m}{b_m} + k_{12})(\frac{a_s}{b_s} + k_{24})\right]^{1/2} \tag{5.17}$$

By selecting the gains k_{ij} subject to the constraints above, the 2-port MSM will be passive and therefore stable for all passive terminations $Z_h(s)$ and $Z_t(s)$. This fulfills the stability goal that was sought.

The PR condition is a sufficient condition for stability for all passive terminations. But is it a necessary condition? Colgate[41] shows that for a 1-port interacting with an arbitrary passive environment, passivity (i.e. the PR test) is also a necessary condition. We know of no proof that covers the situation where the environment is restricted to diagonal 2-port terminations.

5.2 Desired port impedances

The second goal was to select the gains k_{ij} such that the stiffnesses at the master amd slave ports take specified values K_m and K_s respectively. The stiffness at the master port K_m is

$$\frac{T_{mss}}{\Theta_{mss}} = s\frac{T_m(s)}{\Omega_m(s)}\bigg|_{s=0} = s\ Z_m(s)\bigg|_{s=0} = K_m$$

Hence

$$K_m = \frac{a_{0m}}{b_{0m}} = k_{11} - \frac{{k_{13}}^2}{k_{23} + K_t}$$

For the slave port,

$$K_s = \frac{a_{0s}}{b_{0s}} = k_{23} - \frac{{k_{13}}^2}{k_{11} + K_h}$$

Rearranging,

$$k_{11} = K_m - \frac{{k_{13}}^2}{k_{23} + K_t} \tag{5.18}$$

and

$$k_{23} = K_s - \frac{{k_{13}}^2}{k_{11} + K_h} \tag{5.19}$$

The suggested steps in the process for selecting k_{ij} are:

Let

$${k_{13}}^2 = k_{23} k_{11}$$

Then

$$k_{11} = K_m + \frac{{k_{13}}^2}{k_{23} + K_t}$$

$$k_{23} = K_s + \frac{{k_{13}}^2}{k_{11} + K_h}$$

Solving for k_{11} and k_{23} yields:

$$k_{11} = \frac{K_m(1+\frac{K_s}{K_t})}{1-\frac{K_m K_s}{K_t K_h}}$$

$$k_{23} = \frac{K_s(1+\frac{K_m}{K_h})}{1-\frac{K_m K_s}{K_t K_h}}$$

These relationships exhibit two important constraints in our specification of desired port stiffnesses. For $K_h = K_s$ and $K_m = K_t$, i.e., when the operator feels the task stiffness and the task feels the operator stiffness, the computed gains k_{11} and k_{23} will be infinite.

From the stability constraints we recall that:

$$k_{11} \geq 0 \quad and \quad k_{23} \geq 0$$

The specification of the desired port stiffnesses K_m and K_s must thus be constrained by:

$$K_m K_s < K_h K_t \tag{5.20}$$

Therefore, though stability will be guaranteed for any passive termination for non-negative k_{11} and k_{23}, the performance will depend on our estimates of task and operator's stiffnesses during the design stage. If we relate K_m to K_t we get

$$K_m = k_{11} - \frac{k_{23}\ k_{11}}{k_{23} + K_t} = k_{11}\left[1 - \frac{k_{23}}{k_{23} + K_t}\right]$$

For $K_t > 0$, K_m will be positive if and only if k_{11} and k_{23} have the same sign. Also $K_m = 0$ for $K_t = 0$.

This establishes the selection of k_{11} and k_{23}. Consequently

$$k_{13} = (k_{11} k_{23})^{1/2}$$

The remaining gains to be computed are k_{12} and k_{24} (k_{14} is constrained by k_{12} and k_{24}). One way of doing this is to look at the effect that they have on the poles and zeros of the port impedances $Z_m(s)$ and $Z_s(s)$. The following root-locus plots show the effects of each of the gains k_{ij} on the poles and zeros of $Z_m(s)$ (from (5.1)). The values of all but one of the gains are held constant, and trajectories of the poles and zeros are plotted as the one gain is varied. Though the values of k_{12} and k_{24} are selected by inspection, they can be tuned with the help of these plots.

Values of k_{ij} for poles and zeros in the RHS do violate the passivity constraints. For $Z_m(s)$, the poles are functions only of k_{23} and k_{24}. In practice when $k_{23} > 25$ the system became unstable even though the root locus plot for k_{23} indicates stability for values of the gain above 25. It should be emphasized here that the passivity (and consequently the stability) constraints were derived in the s-domain and any translation into the z-domain must be approached with caution.

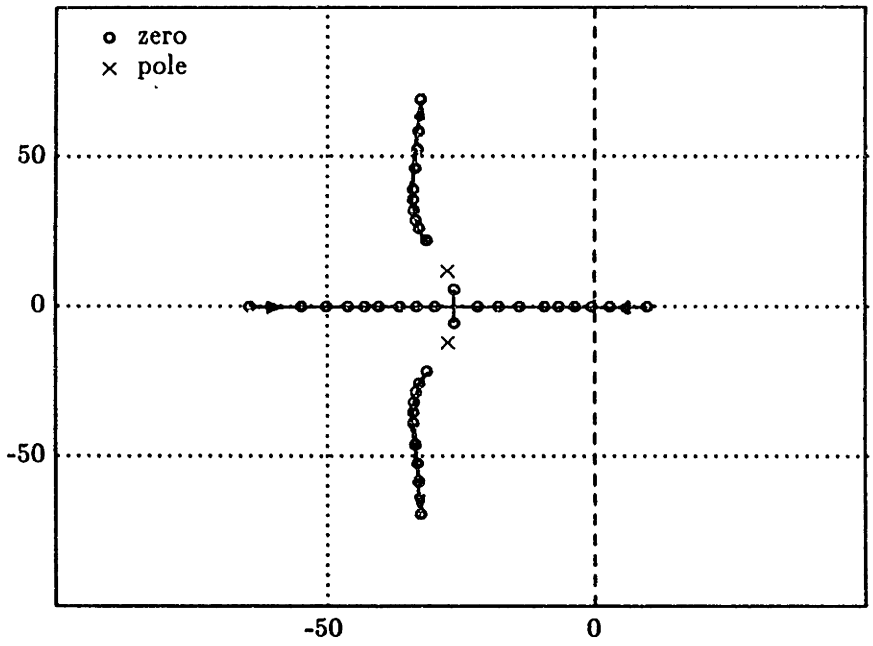

Figure 5.2. Root locus for gain k_{11}

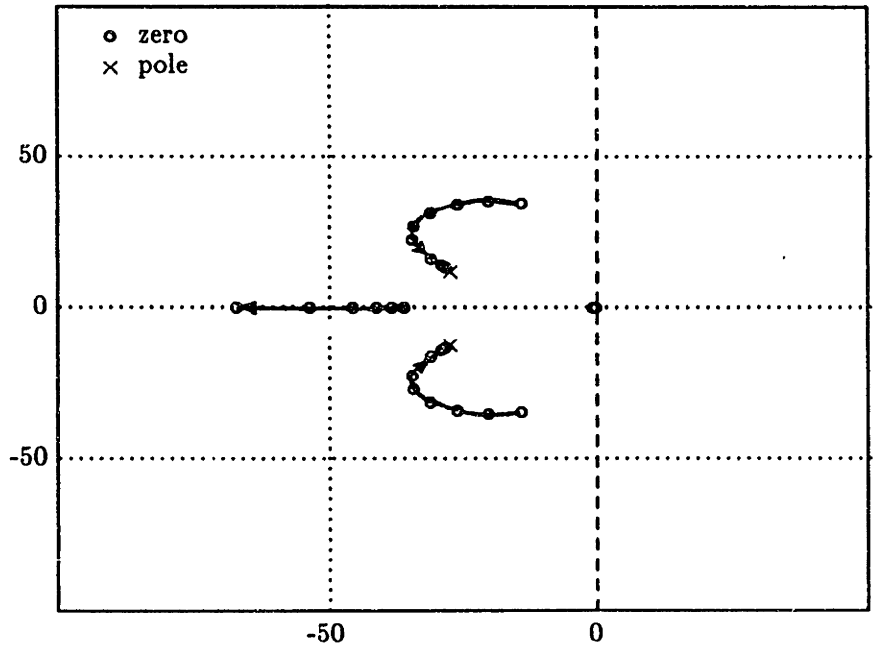

Figure 5.3. Root locus for gain k_{12}

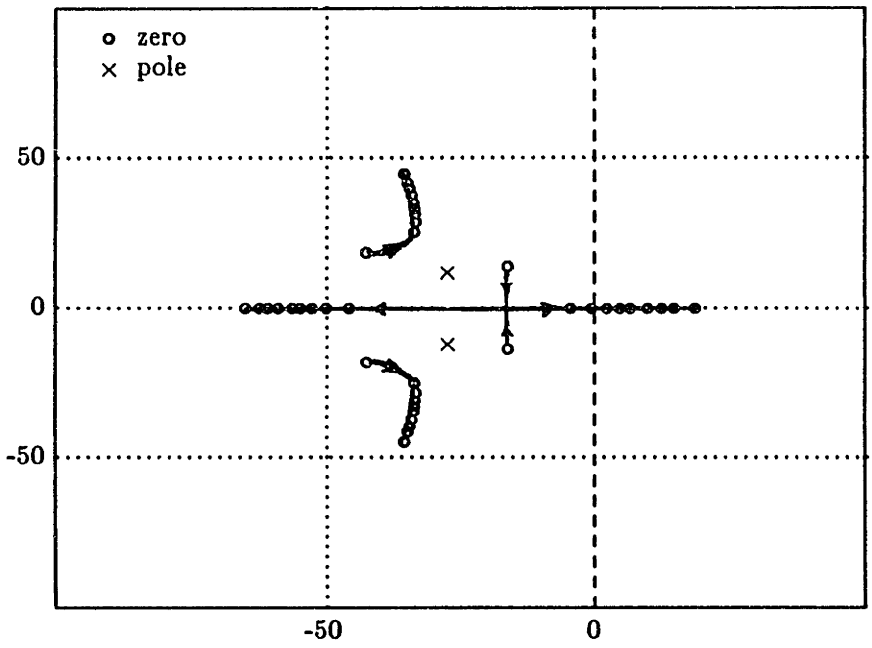

Figure 5.4. Root locus for gain k_{13}

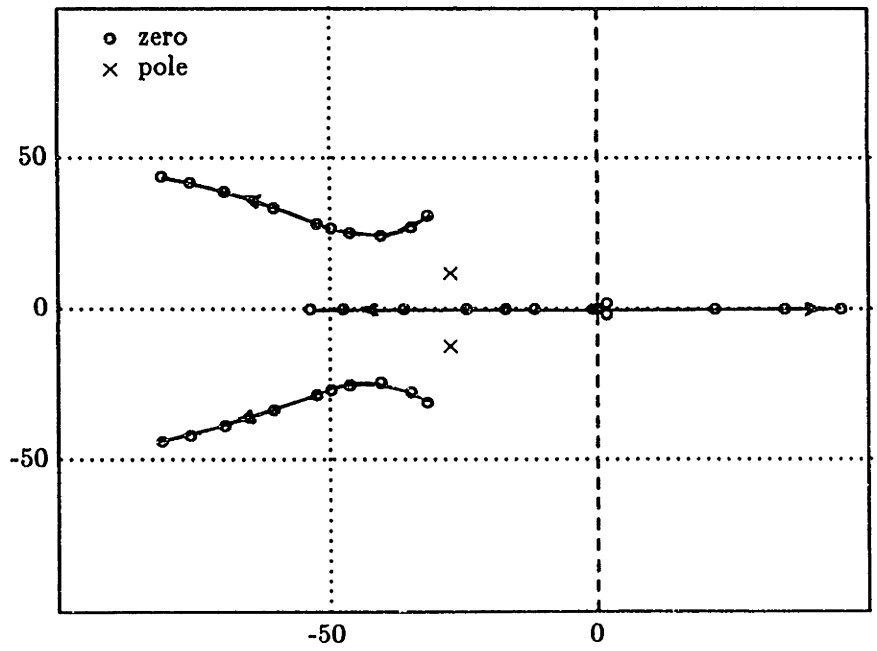

Figure 5.5. Root locus for gain k_{14}

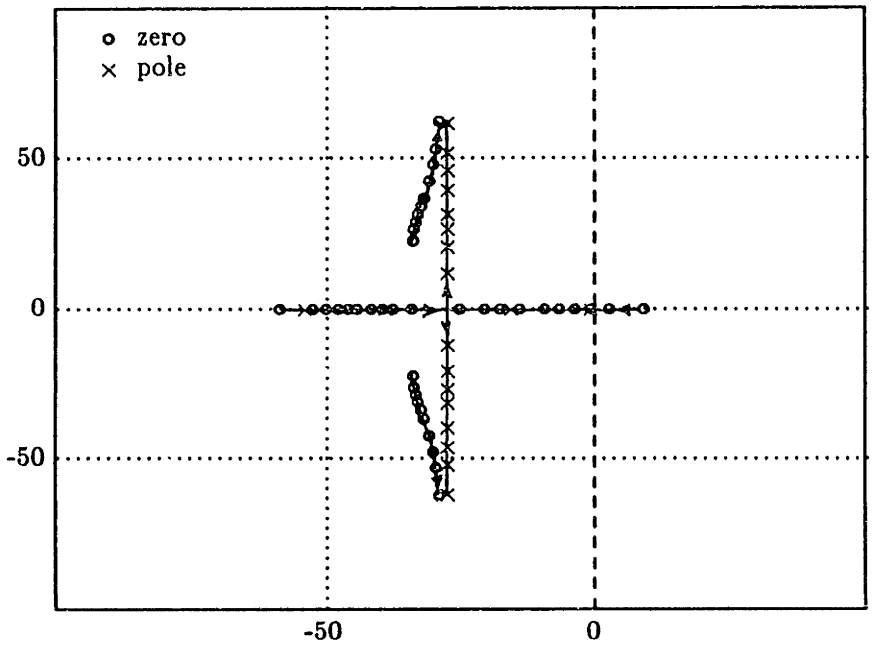

Figure 5.6. Root locus for gain k_{23}

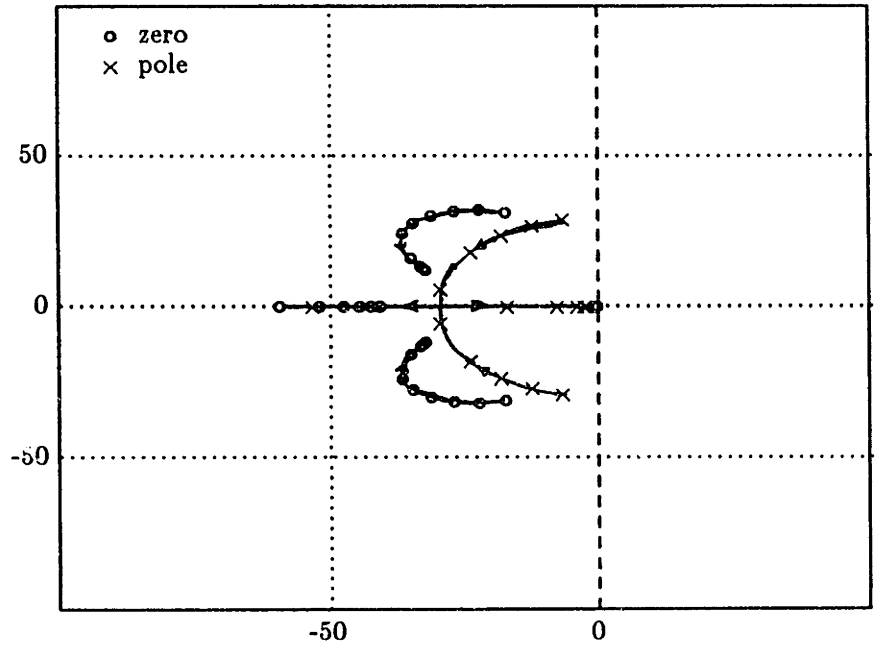

Figure 5.7. Root locus for gain k_{24}

5.3 Human and task impedance parameters

Estimates of the impedance parameters for the models of the human and the task are needed to compute the poles and zeros of the port impedance $Z_m(s)$ for the root locus plots and to find a nominal set of gains based on desired port impedances.

The impedance parameters for the human arm Z_h ($[J_h, B_h, K_h]$) from measurements by Abul-Haj[42] show that for an average adult male the inertia of the forearm about the elbow $\approx 0.06\ N-m-sec^2 = 8.4\ oz-in-sec^2$. The damping ratio ζ_h falls in the range $0.15 < \zeta_h < 1.5$. The stiffness K_h falls in the range $1.0 < K_h < 200\ N-m/rad$ *or* $140 < K_h < 28000\ oz-in/rad$

$$B_h = J_h(2\zeta_h\sqrt{K_h/J_h})$$

The parameters for the experimental task Z_t ($[J_t, B_t, K_t]$) can be estimated from the metal disc and spring that comprise the task. J_t = inertia of the metal disc is $\approx 0.07 oz-in-sec^2$. K_t = stiffness of task is $\approx 1000\ oz-in/rad.$

$$B_t = J_t(2\zeta_t\sqrt{K_t/J_t})$$

6. Experimentation

One of the challenges in conducting an experiment using the apparatus outlined in Chapter 3 is to conceive a single-degree of freedom task that may demonstrate the advantages of an adjustable MSM. If the task execution were repeated for differing combinations of master and slave port impedances (primarily stiffnesses), the effect of these variations could be studied. If the task could be performed equally well over a reasonable range of master and slave port impedances, then one could surmise that for the chosen task, an adjustable MSM does not offer significant advantages. A similar conclusion could be reached if the best combination of impedances comprised the limits of each of the master and slave range of impedances. In other words, if the best performance was always achieved for the combination of highest master and highest slave impedances, or the lowest, then one could argue that providing for other values of the port impedances does not help. If on the other hand, the performance was better at some intermediate combination, a defensible conclusion could be that the particular task is best performed at this combination of master and slave port impedances.

This chapter introduces the task that was selected to be the experimental task, describes the conduct of the experiment, and discusses the resulting data.

6.1 Experimental task

The action of switching a 2-way toggle switch between its two equilibrium positions is a task that humans perform repeatedly with ease. Many such switches are spring-loaded to aid the motion of the contact terminals to their target position and in some cases to provide the operator with tactile feedback during the switch's trajectory. When this mechanism is extended to a multi-position toggle switch the operator has to track the trajectory either visually or by sensing the variations in the spring force between equilibrium positions. The task of switching between adjacent positions of a multi-position spring-loaded switch was chosen as the experiment.

To realize the experimental task in hardware (see Figure 6.2) a half inch thick steel disc was mounted on the slave motor shaft. On the cylindrical face of the disc a hole was drilled to accommodate a spring. A ring was mounted on the motor face chassis concentric to the disc, with 3 sets of 10 set-screws placed radially along the circumference of the ring (see Figure 6.1). The angular separation of the set-screws for the 3 sets were 5, 6, and 7 degrees respectively. A steel ball placed at the tip of the spring in the disc contacted the tips of the set-screws as the disc was rotated inside the ring. In moving from one "valley" (equilibrium position) between a pair of set-screws to an adjacent valley, the spring is compressed as the ball rides over the set-screw tip and released as the it settles into the adajcent valley. By adjusting the depth of the set-screw in the ring, the

extent to which the spring has to be compressed to move the disc through an angular step can be controlled. This manifests itself in the execution of the task as the torque required to step the switch. For the set of 10 screws that were 7 degrees apart, the screw depth was adjusted such that the torque required to switch the disc by one step was much higher (100 oz-ins *vs* 50 oz-ins) than for the set of 10 screws that were 5 degrees apart. The coarse (7 degree) step, high torque switch is designated as Task #1, the fine step (5 degree), low torque switch is designated as Task #2. Experiments were conducted for both tasks.

Four subjects were recruited for the experiments. Each subject was instructed (see Appendix A) to execute the task with eyes closed to block visual feedback of the switch position. In addition the subject was provided with a pair of headphones emanating white noise (inter-station noise in the FM band) to block out the audible click that accompanies the switching action. The task to be executed comprised the action of moving the switch mounted on the slave motor by a single step by manipulating a link (master arm) mounted on the master motor shaft. After an appropriate learning phase the subject was instructed to advance and reverse the switch by a single step 20 times. The 20 cycle process was repeated for 9 combinations of master and slave port stiffnesses (3 levels of master stiffnesses x 3 levels of slave stiffnesses). The entire sequence was repeated for Task #2. The angular position of the slave motor shaft was recorded at every sampling time interval by the computer.

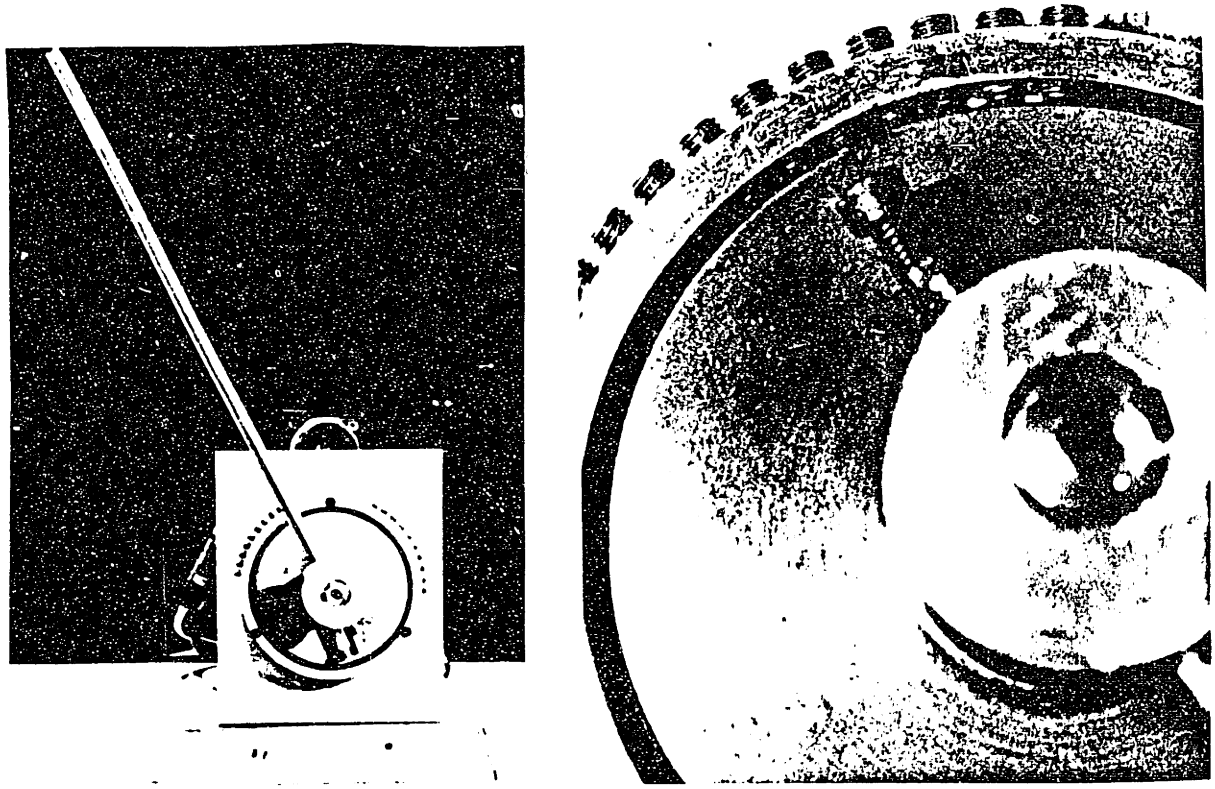

Figure 6.1. Multiposition switch task (detail on right)

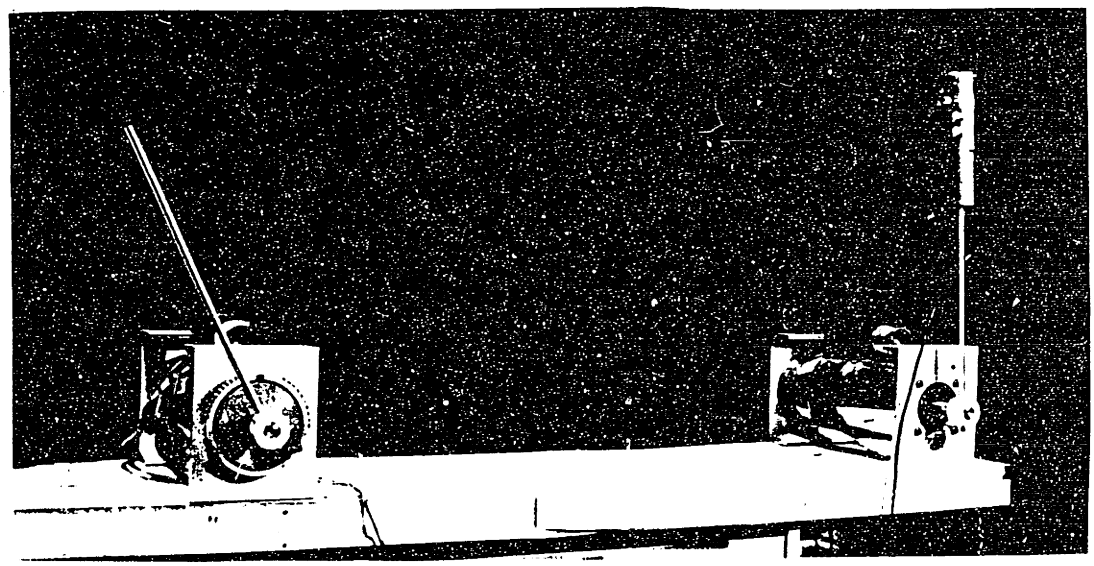

Figure 6.2. Master-Slave system

6.2 Data analysis

The recorded data was then filtered to detect the number of steps that the switch moved and the time taken for each step. Each successful advance by one step and subsequent reversal by one step was counted as one "success" and the time for one step was computed as the average between the advance and reversal. This was necessitated by a lack of symmetry in clockwise and counter-clockwise motions of the switch. The three stifness levels at the master and slave ports are designated as high, medium and low (H,M,L). The maste stiffness always precedes the slave stiffness when a combination is specified, e.g., HM refers to the combination of high master stiffness and medium slave stiffness. The execution time at each combination is designated by t_{ms} where subscript m specifies the master stiffness level (H,M,L) and subscript s specifies the slave stiffness level (H,M,L).

6.2.1 Success rate

The first index computed and analyzed is the number of successful completions of the task goal regardless of the time taken to do so. From the listings in Tables 1 and 2, it is evident (with one aberration for subject #2) that the three levels of master stiffness did not significantly affect the success rate. However it is very clear that at a low slave stiffness the task could rarely if ever be completed successfully. It was observed during the experiment that when the slave stiffness

was low, torque generated by motion of the master arm would build till the slave switched, but with overshoot of an additional step or two. With medium slave stiffness, the success rate drops with decreasing master stiffness for Task #1 and does not change significantly for Task #2.

6.2.2 Task execution time: Sample statistics

The sample mean and standard deviation of the task execution time were computed for each set of successful completions of the task. The sample size for each combination is therefore different. Looking again (Tables 3 and 4) at the effect of master stiffness, t_{HH} and t_{MH} are statistically equal for almost all subjects for both tasks. The same is true for t_{HM} and t_{MM} for Task #2. This appears to indicate that there is a threshold master stiffness level above which no significant improvement in speed is obtained. If we now look at the effect of varying the slave stiffness, for Task #1, t_{XH} is almost always significantly lower than t_{XM} (where X stands for either H, M or L). However for Task #2 this effect is much less pronounced and in some cases the two times are statistically equal. This is not suprising if we recall that for Task #2 the switching torque (the torque required to advance by one step) is lower and can be therefore generated with lower slave port stiffnesses.

Can valid conclusions be drawn from statistics computed from small and unequal sample sets as in this case? To address this concern an alternative

method to compute the sample statistics is used in the next section.

6.2.3 Task execution time: Hypotheses testing

In this method proposed by Mendel[43] the tools of Bayesian statistics are used to compute a posterior distribution of a future measurement of task execution time based on a set of past measurements. If we start with one measurement, an assumed prior distribution can be updated by the measurement to yield the posterior distribution. With every additional measurement this process can be repeated to yield a posterior for the set of measurements of size n. Mendel shows that the parameters of the posterior distribution (mean and variance for a Gaussian model) converge rapidly to the true parameters of the event. This is useful when dealing with small sample sets and when comparing data from sample sets of different sizes. Of particular interest to us is the comparision of data from the task under different combinations of master and slave port stiffnesses. The hypothesis test suggested by Mendel determines with what probability a future measurement from one sequence of data will be greater than another. This measure† is tabulated (Tables 5 and 6) for the six different combinations of master and slave impedances. The elements of the matrix show the probability that the task execution time for the row combination will be lower than the task

† It was computed using an in-house software package developed by Jim Roseborough in the Man-Machine Systems Lab using Mendel's approach.

execution time for the column combination. A probability of 0.5 would suggest that the the next sample of task execution time from each of the two combinations would be equal.

First, let us look at the effect of varying the master stiffness level from H to M to L for Task #1 (Table 5). $P(t_{HH}<t_{MH})$ is close to 0.5 for all four subjects. But $P(t_{MH}<t_{LH})$ and $P(t_{HH}<t_{LH})$ are higher than 0.5 indicating that there is a threshold master stiffness level (probably between M and L) below which the speed of task execution suffers. A similar effect can be seen for Task #2 (Table 6).

If we now study the effect of varying the slave stiffness level for Task #1, $P(t_{HH}<t_{HM})$ is consistently much higher than 0.5. However for Task #2 this effect is much less pronounced, and for two subjects $P(t_{HH}<t_{HM})$ is equal to 0.5, suggesting that the force levels required to execute the task (which are higher for Task #1) determine the suitable level of slave stiffness.

Subject #1 Successes		Slave		
		H	M	L
Master	H	20	19	0
	M	16	13	0
	L	20	11	0

Subject #2 Successes		Slave		
		H	M	L
Master	H	19	11	0
	M	19	16	0
	L	8	5	0

Subject #3 Successes		Slave		
		H	M	L
Master	H	20	19	2
	M	20	13	0
	L	18	19	0

Subject #4 Successes		Slave		
		H	M	L
Master	H	20	19	2
	M	20	14	0
	L	20	8	0

TABLE 1. Task #1 successes

Subject #1 Successes		Slave		
		H	M	L
Master	H	19	20	10
	M	19	17	6
	L	20	20	1

Subject #2 Successes		Slave		
		H	M	L
Master	H	19	3	5
	M	19	8	1
	L	19	18	3

Subject #3 Successes		Slave		
		H	M	L
Master	H	20	19	2
	M	20	20	0
	L	20	19	0

Subject #4 Successes		Slave		
		H	M	L
Master	H	20	17	0
	M	20	20	3
	L	20	19	4

TABLE 2. Task #2 successes

Subject #1		Slave			
		H		M	
		μ	σ	μ	σ
Master	H	1.49	0.48	2.10	0.52
	M	1.57	0.33	1.71	0.45
	L	1.74	0.43	2.78	0.67

Subject #2		Slave			
		H		M	
		μ	σ	μ	σ
Master	H	1.17	0.27	1.67	0.18
	M	1.25	0.52	1.87	0.30
	L	2.54	0.66	3.22	0.74

Subject #3		Slave			
		H		M	
		μ	σ	μ	σ
Master	H	0.66	0.25	1.52	0.19
	M	0.78	0.27	1.20	0.15
	L	1.00	0.50	1.44	0.22

Subject #4		Slave			
		H		M	
		μ	σ	μ	σ
Master	H	1.10	0.12	1.26	0.13
	M	1.12	0.22	1.41	0.31
	L	1.18	0.46	1.82	0.28

TABLE 3. Task #1 sample mean (μ) and standard deviation (σ)

Subject #1		Slave			
		H		M	
		μ	σ	μ	σ
Master	H	0.47	0.04	0.73	0.18
	M	0.55	0.13	0.75	0.26
	L	0.86	0.36	1.14	0.49

Subject #2		Slave			
		H		M	
		μ	σ	μ	σ
Master	H	1.06	0.29	1.22	0.12
	M	1.08	0.25	1.16	0.43
	L	1.46	0.23	1.83	1.14

Subject #3		Slave			
		H		M	
		μ	σ	μ	σ
Master	H	0.98	0.19	0.98	0.10
	M	1.09	0.14	1.02	0.21
	L	1.87	0.37	1.28	0.17

Subject #4		Slave			
		H		M	
		μ	σ	μ	σ
Master	H	0.94	0.31	1.13	0.36
	M	1.06	0.29	1.22	0.50
	L	1.31	0.43	1.52	0.80

TABLE 4. Task #2 sample mean (μ) and standard deviation (σ)

Subject #1 $P(t_i<t_j)$							
		HH	HM	MH	MM	LH	LM
	HH	-	0.68	0.53	0.53	0.59	0.76
	HM	0.32	-	0.35	0.36	0.40	0.63
	MH	0.47	0.65	-	0.51	0.56	0.75
	MM	0.47	0.64	0.49	-	0.55	0.74
	LH	0.41	0.60	0.44	0.45	-	0.71
	LM	0.24	0.37	0.25	0.26	0.29	-
Subject #2 $P(t_i<t_j)$							
		HH	HM	MH	MM	LH	LM
	HH	-	0.65	0.53	0.73	0.77	0.77
	HM	0.35	-	0.40	0.58	0.67	0.70
	MH	0.47	0.61	-	0.69	0.75	0.75
	MM	0.27	0.42	0.31	-	0.62	0.66
	LH	0.23	0.33	0.25	0.38	-	0.56
	LM	0.22	0.30	0.24	0.34	0.44	-
Subject #3 $P(t_i<t_j)$							
		HH	HM	MH	MM	LH	LM
	HH	-	0.81	0.55	0.69	0.62	0.79
	HM	0.19	-	0.22	0.37	0.31	0.47
	MH	0.45	0.78	-	0.65	0.58	0.76
	MM	0.31	0.63	0.35	-	0.44	0.60
	LH	0.38	0.69	0.42	0.56	-	0.66
	LM	0.21	0.53	0.24	0.40	0.34	-
Subject #4 $P(t_i<t_j)$							
		HH	HM	MH	MM	LH	LM
	HH	-	0.57	0.51	0.60	0.53	0.67
	HM	0.43	-	0.44	0.54	0.47	0.63
	MH	0.49	0.56	-	0.59	0.52	0.66
	MM	0.40	0.46	0.41	-	0.44	0.59
	LH	0.47	0.53	0.48	0.56	-	0.64
	LM	0.33	0.37	0.33	0.41	0.36	-

TABLE 5. Task #1 Hypothesis test

Subject #1 $P(t_i<t_j)$							
		HH	HM	MH	MM	LH	LM
	HH	-	0.61	0.53	0.61	0.66	0.74
	HM	0.39	-	0.42	0.51	0.56	0.65
	MH	0.47	0.58	-	0.59	0.63	0.71
	MM	0.39	0.49	0.42	-	0.54	0.64
	LH	0.34	0.44	0.37	0.46	-	0.60
	LM	0.26	0.35	0.29	0.36	0.40	-
Subject #2 $P(t_i<t_j)$							
		HH	HM	MH	MM	LH	LM
	HH	-	0.50	0.51	0.53	0.66	0.69
	HM	0.50	-	0.50	0.52	0.59	0.64
	MH	0.49	0.50	-	0.52	0.65	0.68
	MM	0.47	0.48	0.48	-	0.59	0.65
	LH	0.34	0.40	0.35	0.41	-	0.60
	LM	0.31	0.36	0.32	0.35	0.40	-
Subject #3 $P(t_i<t_j)$							
		HH	HM	MH	MM	LH	LM
	HH	-	0.50	0.55	0.52	0.81	0.63
	HM	0.50	-	0.55	0.52	0.82	0.63
	MH	0.45	0.45	-	0.46	0.79	0.59
	MM	0.48	0.48	0.53	-	0.80	0.61
	LH	0.19	0.18	0.21	0.20	-	0.30
	LM	0.37	0.37	0.41	0.39	0.72	-
Subject #4 $P(t_i<t_j)$							
		HH	HM	MH	MM	LH	LM
	HH	-	0.57	0.55	0.60	0.64	0.68
	HM	0.43	-	0.47	0.53	0.57	0.62
	MH	0.45	0.53	-	0.56	0.60	0.64
	MM	0.40	0.47	0.44	-	0.53	0.59
	LH	0.36	0.43	0.40	0.47	-	0.57
	LM	0.32	0.38	0.36	0.41	0.43	-

TABLE 6. Task #2 Hypothesis test

6.3 Discussion of experimental results

What reasonable conclusions can one draw from the experimental data for this task? From the viewpoint of success and speed, the combination of high master stiffness and high slave stiffness satisfies both goals. However, the success rate, the sample statistics, and the hypothesis test indicate that equally good results can be obtained at a lower level of master stiffness. If the performance measure was based only on success in executing the task, all three levels of master stiffness are adequte. At the lowest level the speed of execution appears to suffer a little. The effect of master stiffness on task performance is very similar for both tasks, indicating perhaps that selection of the master port stiffness is independent of the task stiffness.

A different picture emerges for the slave port stiffness selection. It is apparent (and not unexpected) that the stiffness level selected at the port where the interaction with the task occurs is related to the task characteristics. As a consequence, the effect of varying the slave stiffness is different for the two tasks, and is indicated both by the sample statistics and the hypothesis test. The task (#2) which required a lower torque to complete the switching action did not suffer much in execution speed when the slave stiffness level was decreased. Since the stiffness level at the slave port determines the force level that can be generated at the port, it is not suprising that at a very low level neither task could be executed successfully.

7. Summary and conclusions

We started with a hypothesis that humans tend to adjust their own impedance when interacting with their enviornment. As a consequence we suggested that it would be natural to extend this capability to a tool used to interact with a remote enviornment. A model and a framework for a design procedure to achieve this goal were presented. The design was realized in hardware by a one degree of freedom Master-Slave Manipulator. Using this apparatus, an experiment was conducted to check if the capability to adjust the impedance parameters of the MSM was gainful.

It would be both foolish and pretentious to reach definitive conclusions based on a single task. However, there are some interesting observations that can be made in a qualitative sense. The level of force-feedback that the operator feels is determined by the specification of the master port impedance. Force-feedback is useful in interacting with remote tasks upto a certain level, beyond which a performance index based on speed and success of task execution will not improve significantly. If other criteria such as operator fatigue, comfort and arm strength (a low force-feedback level would allow a weak operator to compress a stiff spring) are factored into the performance index, there is no apparent reason to believe that the highest level of force-feedback would be the best.

The experiment clearly established that the selection of the slave port impedance is dependent on the task characteristics. Hence a reasonable

conclusion that can be reached is that the capability to adjust the impedances of the MSM is advantageous in executing tasks with widely differing characteristics or tasks that are made up of sub-tasks that have differing characteristics. Before contact with the task object the slave port impedance should be low, and the master port impedance high, so that contact can be sensed but not result in the imposition of excessive force on the task object. Upon contact, the slave port impedance should be increased so that the task can be executed, and the master port impedance reduced to provide a comfortable but adequate level of force-feedback to the operator. The functional dependence of the impedances selected on the characteristics of the operator and the task is an area that can be explored further with the aid of design tools that have been developed in this dissertation.

7.1 Suggestions for further research

The first extension to this thesis that I would suggest is to expand the parameters that are varied in the experiment. What would the effect be of using a stiffer spring in the switch? Would visual feedback of the task affect the selection of port impedances? Next, other single degree of freedom tasks with differing characteristics in terms of task impedances should be designed.

The 2-port network can be made more general by removing the reciprocity condition that I chose to impose for the sake of simplicity. What additional flexibility would be gained by this is an open question. The other constraint that

could be loosened is the specification of only the stiffness component of the port impedances. The desired port impedances can be specified as second-order network functions with desired inertia, damping and stiffness components. Deriving design rules for the selection of gains to meet the desired impedances rather than simply desired stiffnesses may be more complex.

If one were to discover an "optimal" slave port impedance for a particular task, it would be interesting to study the relationship between the "optimal" port impedance and the impedance of the task. It is known that power is most efficiently transmitted across the port when the port impedance and the termination impedance are equal. Whether the selection of the slave port impedance to match the task impedance also results in the best performance needs to be investigated.

One of the problems when the operator and the task are separated by a large distance is the delay in the transmission of signals back and forth. This delay time, also called transportation lag, is a non-minimum phase element which renders the system transfer functions non-minimum phase and invalidates many of the concepts that have been adopted in the development of the stability and gain selection procedures.

Another substantial extension to this work would involve developing a design methodology for a general six degree of freedom MSM. If it is possible to decouple the 6-DOF MSM into single DOF linear sub-systems, the procedure

shown in this thesis can be applied to each linear subsystem to design a 6-DOF adjustable MSM. A framework within which a specification of desired port impedances in all six degrees of freedom could be made (consider that one would have to specify three terms, inertia, damping, and stiffness, for each of the six degrees of freedom, at each of the two ports, for a total of 36 terms) would by itself be an important contribution.

Appendix A

Instructions to subject for experiments

The task that you are asked to perform is the action involved in moving a multi-position rotary switch between adjacent detente points. You will attempt this task not by handling the switch directly but through an interface that provides you with some feedback of the forces that are encountered in moving the switch between adjacent detente points. You will see one lever with a black handle grip mounted on one motor shaft. This is the lever that you will move to attempt the task. The second motor that you see with a lever mounted on its shaft is directly connected to the rotary switch. Please follow the steps outlined below to guide you before and during the experiment.

- By moving the lever connected directly to the rotary switch, get a feel of the task when you perform the action of switching between adjacent points. You will hear an audible click and feel a relaxation of the switch spring force when the switch rotor advances to the next point.
- Place the headphones provided over your ears and adjust the volume of the white noise you hear till you can no longer hear the clicking action of the switch.
- When prompted to do so grip the black handle and attempt to move the lever to switch back and forth between adjacent positions. If you cannot feel any forces from the switching action please let me know.
- You can take a few minutes to play around to get a feel of what the task is and ask for any clarifications.
- When you are ready, MAKE SURE THE HEADPHONES ARE ON, and await a visual "thumbs up" prompt from me.
- Upon the prompt, close your eyes and attempt to advance the switch counter-clockwise by ONE STEP ONLY, and then reverse it clockwise by ONE STEP ONLY, and repeat the process 20 times, counting loudly so that I can hear you. Each advance and reversal counts as ONE action. You must therefore alternate 20 advances with 20 reversals. You must perform the action at as fast a pace as you feel comfortable with in accomplishing the objective of switching by ONE STEP ONLY.
- At the completion of each sequence, I will do some housekeeping and prompt ("thumbs up") you for the next sequence, whereupon you will repeat the actions above.

- The entire experiment will consist of at least 2 sets of 9 of the above sequences, and at most 6 sets.
- Should any of the following events occur during an experiment, please act according to the prescription below:
    - If you sense that you have moved by MORE THAN ONE STEP proceed without stopping as if you had advanced by only one step.
    - If you can no longer sense any forces or are fatigued or uncomfortable, abort the task by alerting me.
    - If I have to abort the task for any reason whatsoever I will let you know by tapping lightly on your shoulder (remember your eyes are closed during the task).
- Thank you for your help and patience and spirit of goodwill.

Appendix B

System hardware diagrams

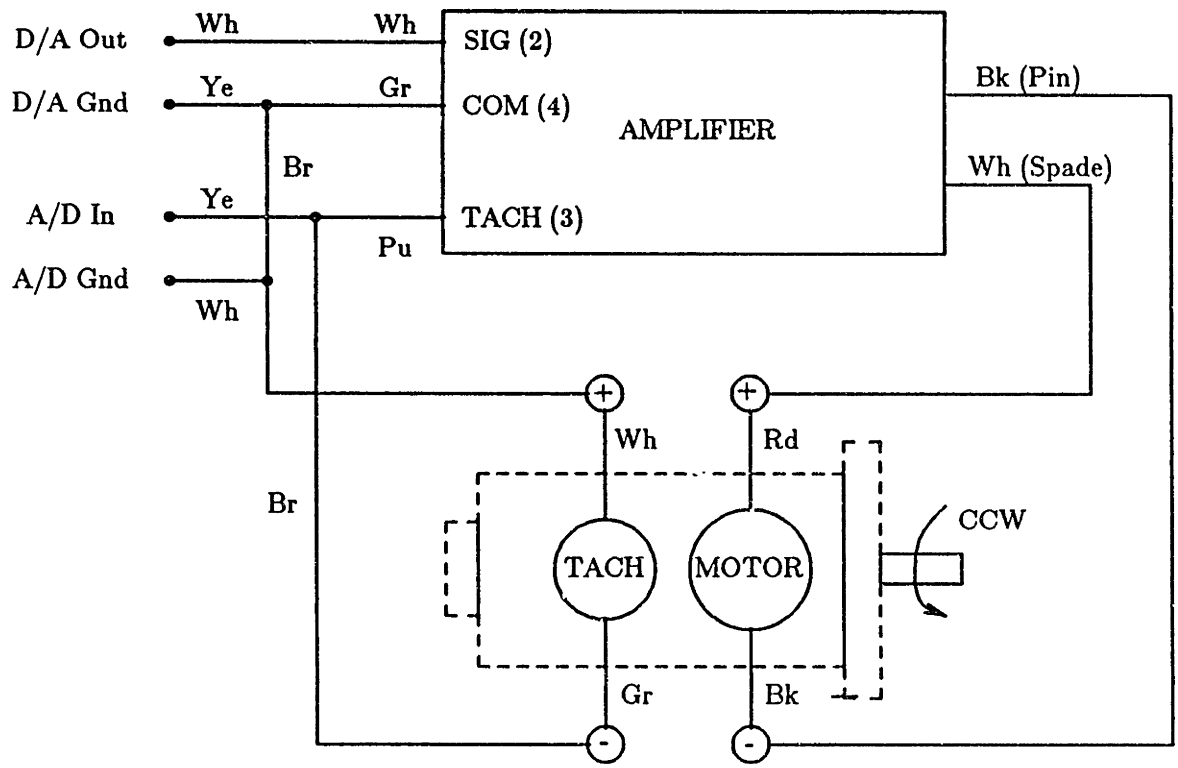

Figure B.1. Motor-Tach connections

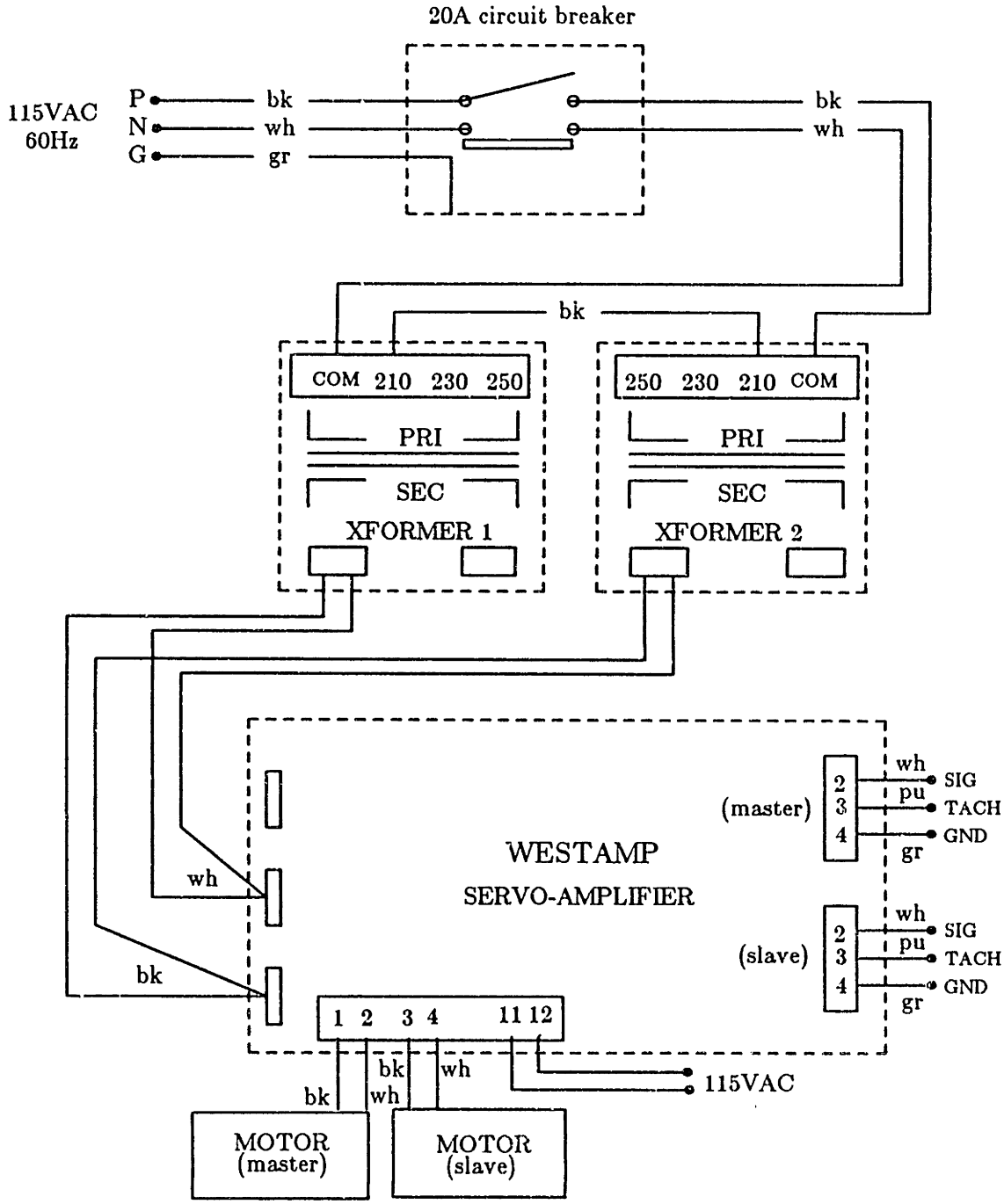

Figure B.2. Power connections to servo-amplifier

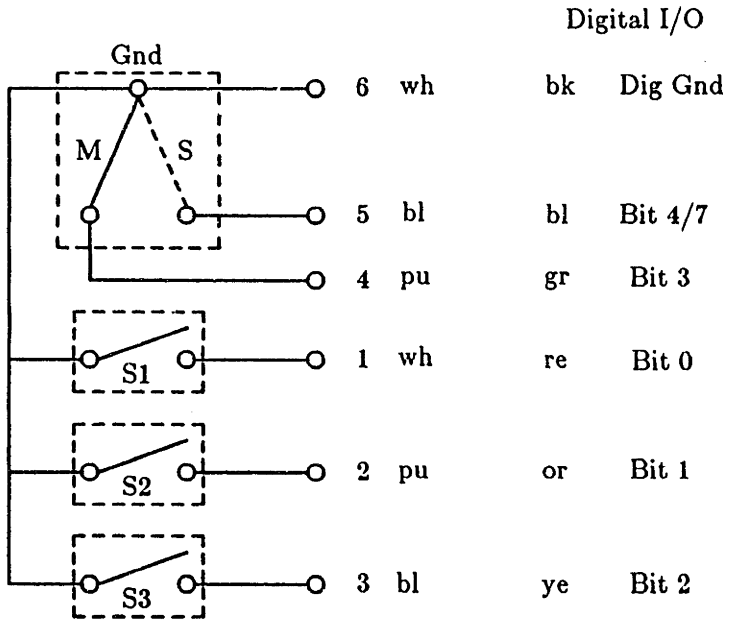

Figure B.3. Schematic of control handle switches

DE9 Plug at Computer		Signal	DE9 Plug at Motor	
Pin	Color		Pin	Color
1	*White*	A	1	*Brown*
2	*Black*	INV-A	2	*White*
3	*Yellow*	B	3	*Yellow*
4	*Black*	INV-B	4	*Green*
5	*Red*	+5V	5	*Red*
9	*Black*	GND	9	*Black*
-	*Green*	-Vel*	8	*Green*
-	*Black*	+Vel*	7	*White*
6	*Blue*	INDEX	6	*Blue*

* (for CCW rotation of motor shaft)

Data acquisition board connections							
Board		DE9 Plug		Amplifier		DIN Plug	
Signal	Color	Color	Pin	Color	Pin	Pin	Signal
A/D Ch	*Yellow*	*Green*	8	*Purple*	3	-	-
A/D Gnd	*White*	*Black*	7	-	-	-	-
D/A Ch	*White*	-	-	*White*	2	-	-
D/A Gnd	*Yellow*	-	-	*Green*	4	-	-
Bit 0	*Red*	-	-	-	-	1	*Switch 1*
Bit 1	*Orange*	-	-	-	-	2	*Switch 2*
Bit 2	*Yellow*	-	-	-	-	3	*Switch 3*
Bit 3	*Green*	-	-	-	-	4	*Switch M*
Bit 4	*Blue*	-	-	-	-	5	*Switch S*
Dig Gnd	*Black*	-	-	-	-	6	*Gnd*

Figure B.4. Motor-Computer-Amplifier connections

Appendix C

Encoder interface card and clock

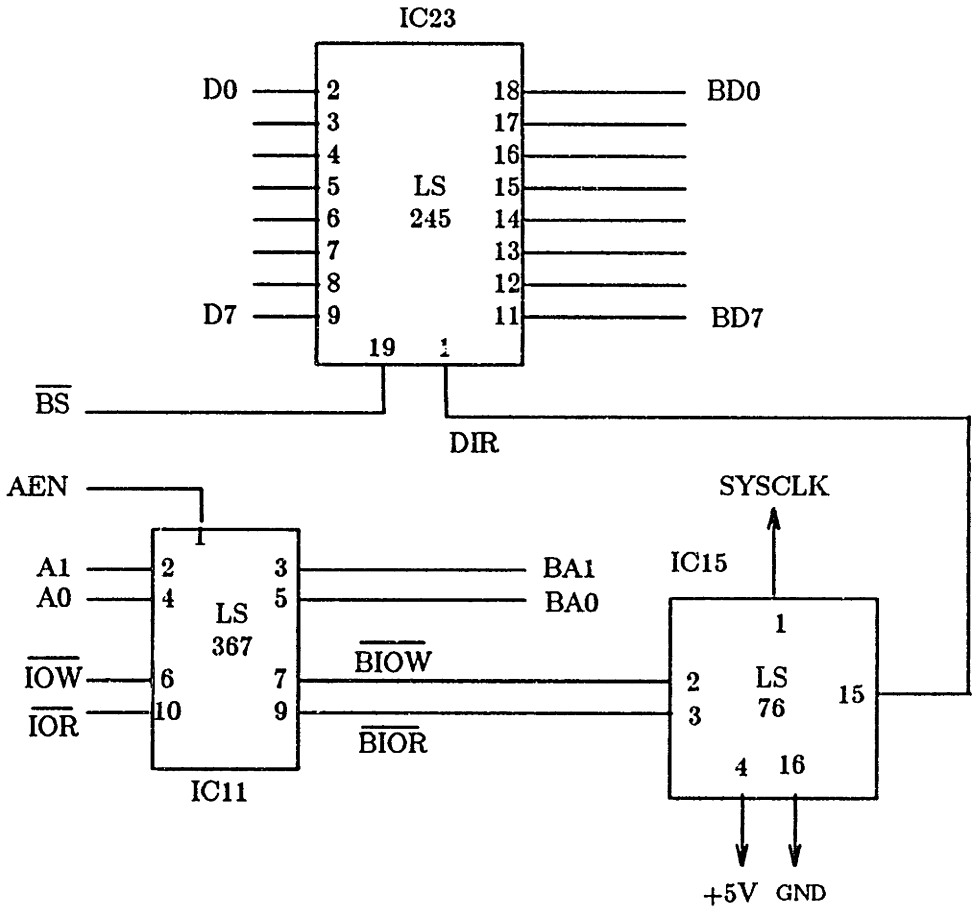

Figure C.1. Data bus interface

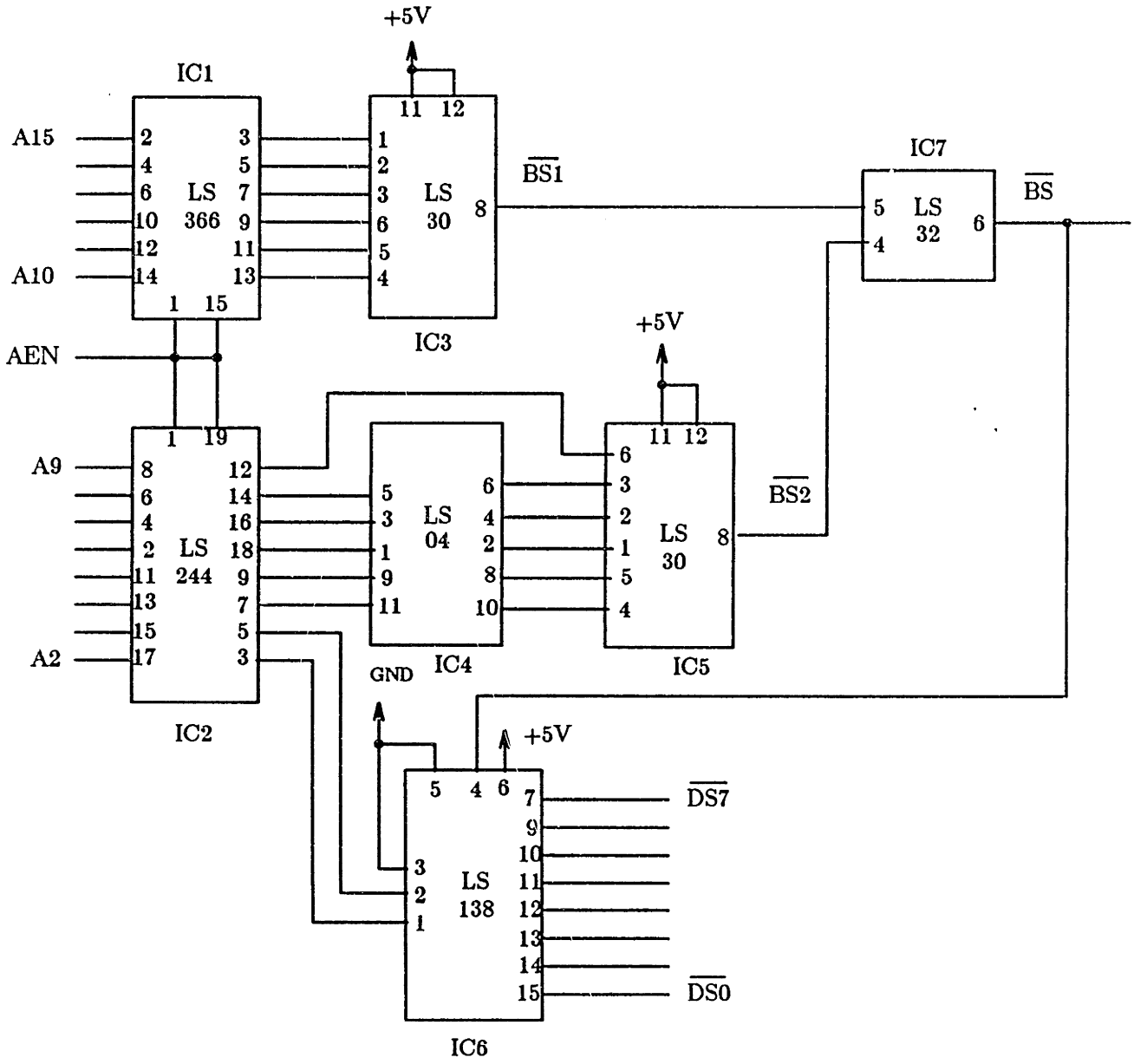

Addresses: 0200H-020FH

Figure C.2. Device address selection

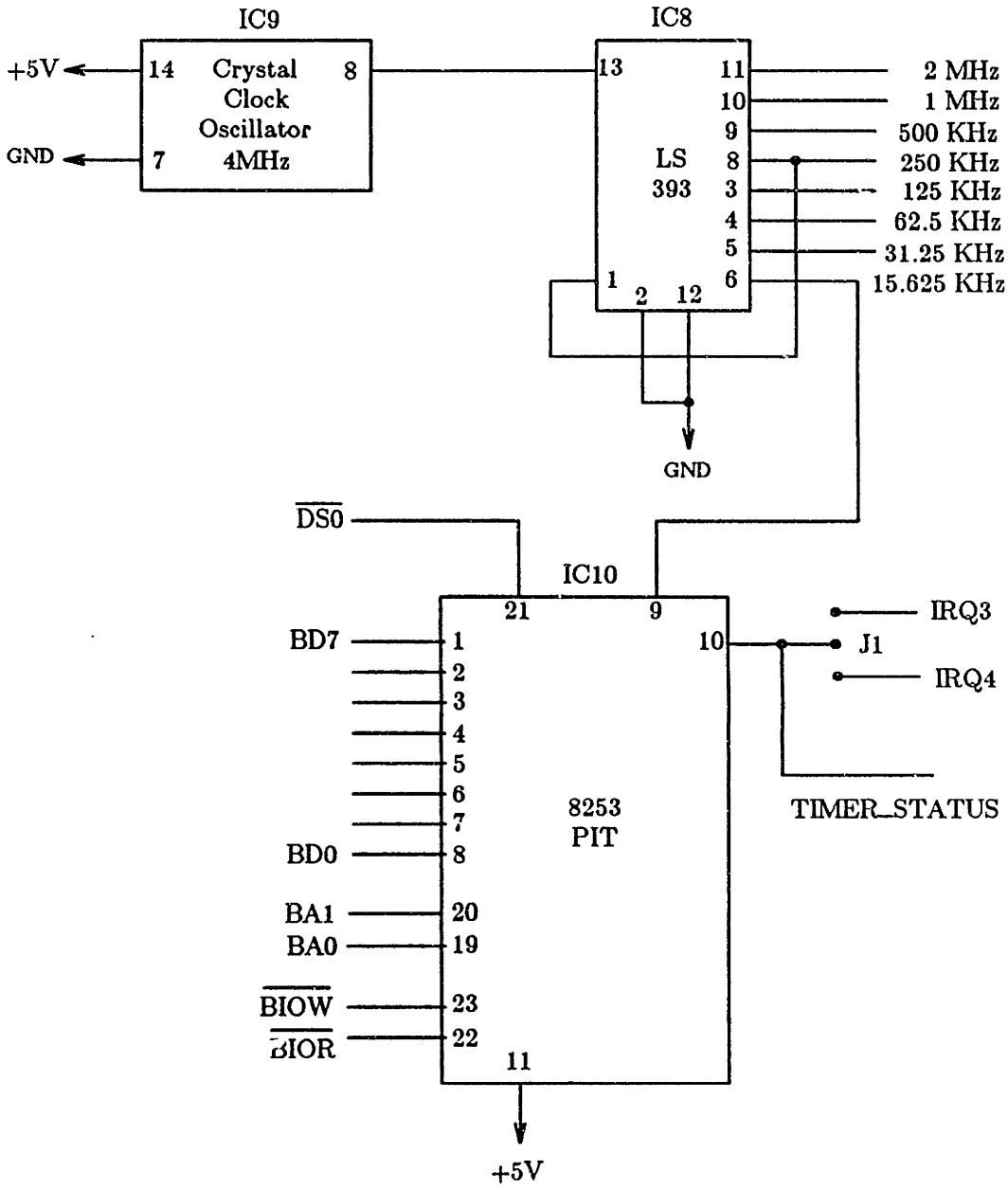

Figure C.3. Real-time clock

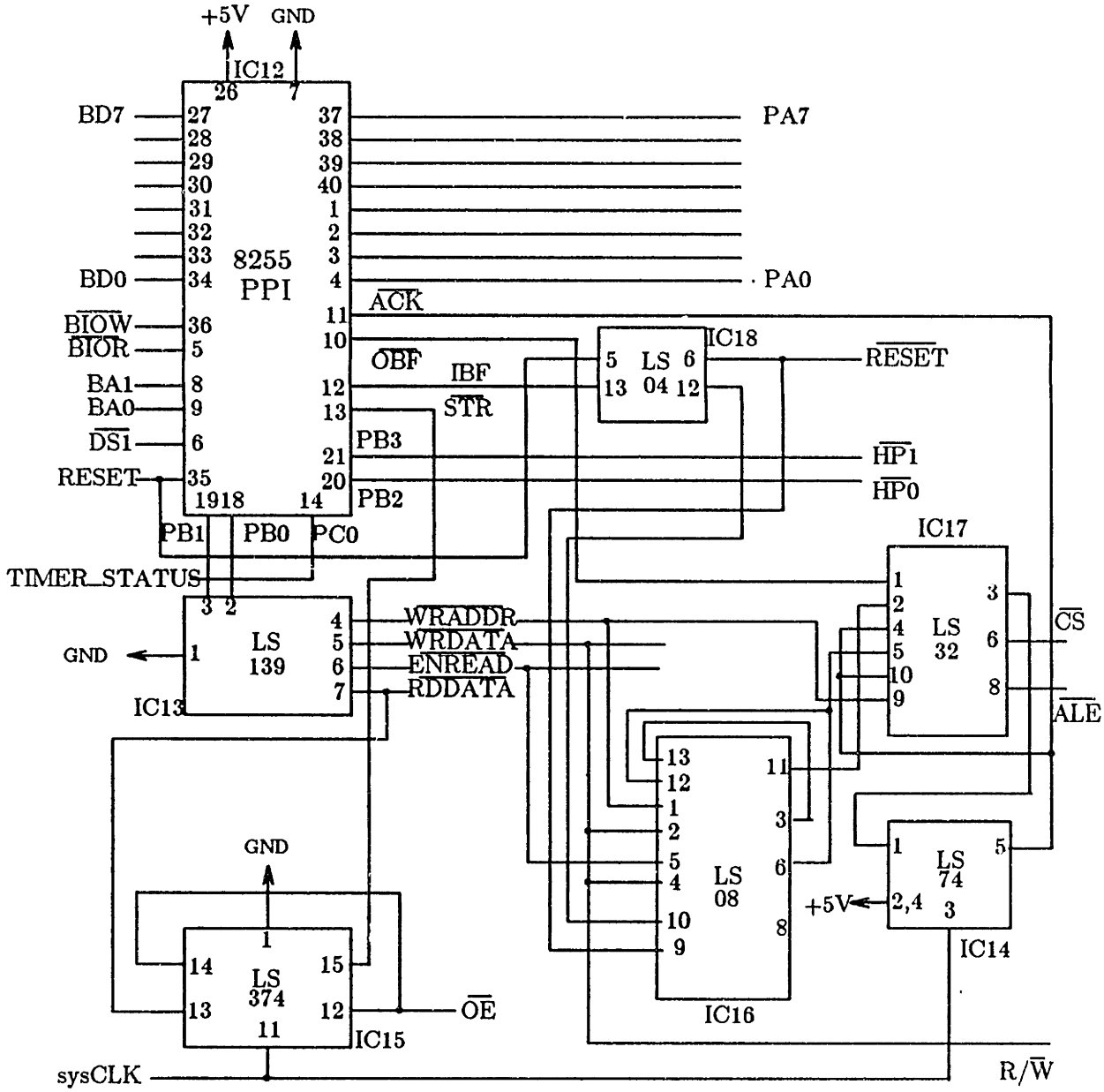

Figure C.4. Programmable peripheral interface

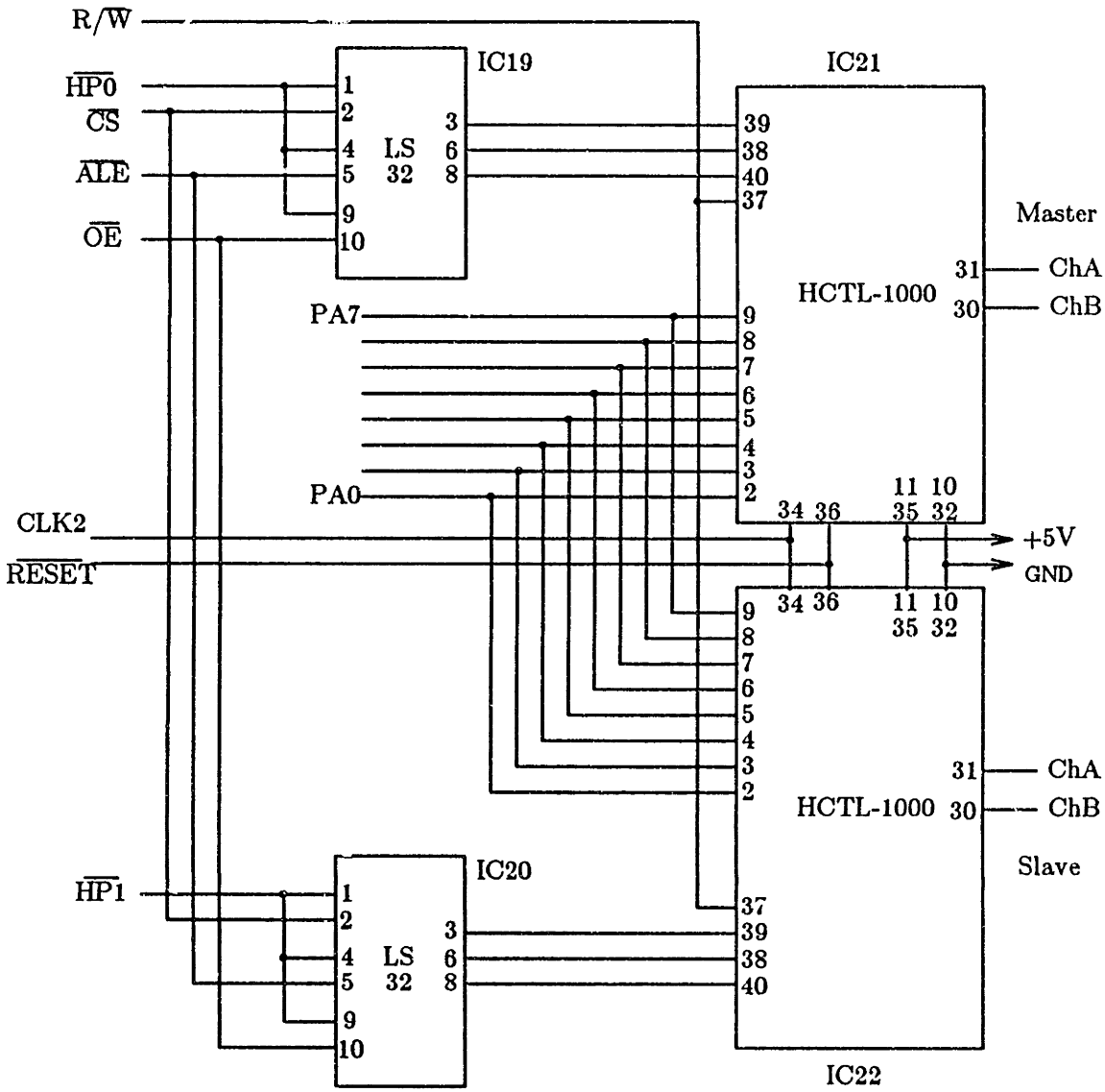

Figure C.5. HP Motion controllers

REFERENCES

1. Goertz, R.C., *Nucleonics*, Vol. 10, No. 11 (1952), p. 36

2. Jelatis, D.G., Design Criteria for Heavy-Duty Master Slave Manipulators. In *Proc. of the 7th Hot Lab and Eqpt Conf.*. American Nuclear Society, Cleveland, Ohio, April, 1959.

3. Johnson, E. G. and Corliss, W. R., Teleoperators and Human Augmentation, An AEC-NASA Technology Survey, NASA SP-5047, December 1967.

4. Ballard, R. D., ROV Development at Woods Hole's Deep Submergence Laboratory, Marine Technology Society Meeting on Remotely Operated Vehicles, San Diego, May 1984.

5. Ceppolina, F., et al., Extravehicular Activity Annex: Solar Max Repair Mission. *NASA JSC Document No. 14082, Annex 11, Rev. A,* March 1984.

6. Jenkins, L. Space Telerobotic Systems: Applications and Concepts. In *Proceedings of the Workshop on Space Telerobotics*, Volume 1. JPL Publication 87-13, July 1987.

7. Fischer, G. Telerobotic Assembly of Space Station Truss Structure. In *Proceedings of the Workshop on Space Telerobotics*, Volume 1. JPL Publication 87-13, July 1987.

8. Chun, W. and Cogeos, P. Shuttle Bay Telerobotics Demonstration. In *Proceedings of the Workshop on Space Telerobotics*, Volume 1. JPL Publication 87-13, July 1987.

9. Telepresence Work Station System Definition Study - Part II, TWS Final Report (MCR-86-528,NAS9-17230), May 1987, Martin Marietta Denver Aerospace, Denver, Colorado.

10. Final Report for Telerobotic Work System. Volume 1 - Executive Summary, Report No. SA-TWS-87-R002, April 1987, Grumman Space Systems, Bethpage, NY.

11. Mason, M. T., Compliance and Force Control for Computer Controlled Manipulators. *IEEE Transactions on Systems, Man, and Cybernetics*, Vol SMC-11, No.6, June 1981

12. Hogan, N., Impedance Control: An Approach to Manipulation: Parts I,II,III. *Journal of Dynamic Systems, Measurement, and Control*, 107:1-24, March 1985

13. Salisbury, J. K., Active Stiffness Control of a Manipulator in Cartesian Coordinates. In *19th IEEE Conf on Decision and Control*, Albuquerque, NM, Dec, 1980

14. Kazerooni, H. K., A Robust Design Method for Impedance Control of Constrained Dynamic Systems, Ph.D. Thesis, M.I.T. Department of Mechanical Engineering, Feb 1985

15. Kazerooni, H.K., Robust, Nonlinear Impedance Control for Robot Manipulators, In *Proceedings of the IEEE International Conference on Robotics and Automation*,pages 741-750, 1987

16. Anderson, R. J. and Spong, M. W., Hybrid Impedance Control of Robotic Manipulators, In *Proceedings of the IEEE International Conference on Robotics and Automation*, pgs 1073-1080, 1987.

17. Bejczy, A. and Salisbury, J. K., Kinesthetic Coupling Between Operator and Remote Manipulator, In *Proceedings of the International Computer Technology Conference*, ASME Century 2, Vol 1., San Francisco, CA, Aug 1980, pgs 197-211

18. Handlykken, M. and Turner, T., Control System Analysis and Synthesis for a Six Degree-of-freedom Universal Force-reflecting Hand Controiler, In *Proceedings of the IEEE Conference on Decision and Control*, 1980

19. Arai, T. and Nakano, E., Bilateral Control for Manipulators with Different Configurations, In *Proceedings of IECON* 1984, Vol.1, pgs 40-45.

20. Inoue, H., Computer Controlled Bilateral Manipulator. *Bulletin of the JSME*, Vol14, No.69, 1971, pgs 199-207.

21. Goto, T, Inomaya, T. and Takeyasu, K., Precise Insert Operation by Tactile Controlled Robot, Central Research Laboratory of Hitachi Ltd., Kokubunji, Tokyo, Japan

22. Komada, S., Inamada, S. and Ohnishi, K., Bilateral Robot Hand Based on Estimated Force Feedback, In *Proceedings of IECON* 1987, pgs 602-607.

23. Vertut, J., Fournier, R., Espiau, B. and Andre, G., Advances in a Computer Aided Bilateral Manipulator System, Presented at a Topical Meeting: "Robotics and Remote Handling in Hostile Environments", Gatlinburg, TN, USA, 1984

24. Vertut, J., Advances in Computer Aided Teleoperation Systems (CATS), 1983 ICAR, Tokyo, Japan.

25. Vertut, J., Hugon, R., Fournier, R., Espiau, B. and Coiffet, Ph., Human Factor Aspects of Computer Enhanced Teleoperation, American Nuclear Society, 1983 Annual Meeting, Detroit, USA.

26. Yokokohji, Y. and Yoshikawa, T., Analyis of Maneuverability and Stability for Master-Slave System, Automation Research Laboratory, Kyto University, Uji, Kyoto, Japan.

27. Hill, J. W., Study of Modeling and Evaluation of Remote Manipulation Tasks with Force Feedback, SRI Project 7696 Final Report, March 1979, SRI International, Menlo Park , CA, 94025

28. Bejczy, A. K. and Handlykken, M., Experimental Results with a Six Degree-of-Freedom Force Reflecting Hand Controller, In *Proceedings of the 17th Annual Conference on Manual Control*, UCLA, Los Angeles, CA, June 1981

29. Aidley, D.J., The Physiology of Excitable Cells, 2nd Edition, Cambridge University Press, 1978

30. Oman, C. K., Lecture Notes: Quantitative Physiology: Sensory and Motor Systems, Massachusetts Institute of Technology, Cambridge, Mass, USA.

31. Bahler, A.S., Modelling of Mammalian Skeletal Muscle, In *IEEE Trans on Bio-Medical Engg.* BME-15(4):249-257, Oct, 1968.

32. McRuer, D.T., Magdeleno, R.E., and Moore, G.P., A Neuromuscular Actuation System Model, In *IEEE Trans on Man-Machine Systems* MMS-9(3):61-71, Sep, 1968.

33. Desoer, C. A. and Kuh, E.S., Basic Circuit Theory, McGraw-Hill Book Co., New York, 1969

34. Hayt, W. H. and Kemmerly, J. E., Engineering Circuit Analysis, 4th ed., McGraw-Hill Book Co., New York, 1986.

35. Strum, R. D. and Ward, J. R., Electric Circuits and Networks, 2nd ed., Prentice-Hall Inc, Englewood Cliffs, New Jersey, 1985.

36. Chen, Wai-Kai, Passive and Active Filters, Theory and Implementations, John Wiley & Sons, Inc. 1986.

37. Van Valkenburg, M. E., Introduction to Modern Network Synthesis, Wiley, New York, 1960.

38. Daryanani, Govind, Principles of Active Network Synthesis and Design, John Wiley & Sons, Inc. 1976.

39. Ghausi, M.S., Principles and Design of Linear Active Circuits, McGraw-Hill, Inc. 1965.

40. Mitra, S.K., Analysis and Synthesis of Linear Active Networks, John Wiley & Sons, Inc. 1969.

41. Colgate, J. E., The Control of Dynamically Interacting Systems, Sc.D. Thesis, Aug 1988, M.I.T. Department of Mechanical Engineering, Cambridge, MA.

42. Abul-Haj, C., The Design of an Elbow Prosthesis Simulator for Testing Neurophysiologically Based Controllers, In *Proceedings of the 5th Annual Conference on Rehabilitation Engineering*, Houston, Texas, 1982.

43. Mendel, M. B., Prediction of Spin Symmetric Sequences, Man-Machine Systems Lab Internal Memorandum, M.I.T., Cambridge, MA, USA.